


Stable carbon isotope values of syndepositional carbonate spherules and micrite record spatial and temporal changes in photosynthesis intensity

Mingfei Chen¹  | Jessica L. Conroy^{1,2}  | Emily C. Geyman³  | Robert A. Sanford¹ | Joanne C. Chee-Sanford^{4,5} | Lynn M. Connor^{4,5}

¹Department of Geology, University of Illinois at Urbana-Champaign, Urbana, Illinois, USA

²Department of Plant Biology, University of Illinois at Urbana-Champaign, Urbana, Illinois, USA

³Division of Geological and Planetary Sciences, California Institute of Technology, Pasadena, California, USA

⁴Department of Natural Resource and Environmental Science, University of Illinois at Urbana-Champaign, Urbana, Illinois, USA

⁵USDA-ARS, Urbana, Illinois, USA

Correspondence

Mingfei Chen, Department of Geology, University of Illinois at Urbana-Champaign, Urbana, IL 61801, USA.
Email: mingfei2@illinois.edu

Funding information

American Chemical Society; National Science Foundation

Abstract

Marine and lacustrine carbonate minerals preserve carbon cycle information, and their stable carbon isotope values ($\delta^{13}\text{C}$) are frequently used to infer and reconstruct paleoenvironmental changes. However, multiple processes can influence the $\delta^{13}\text{C}$ values of bulk carbonates, confounding the interpretation of these values in terms of conditions at the time of mineral precipitation. Co-existing carbonate forms may represent different environmental conditions, yet few studies have analyzed $\delta^{13}\text{C}$ values of syndepositional carbonate grains of varying morphologies to investigate their origins. Here, we combine stable isotope analyses, metagenomics, and geochemical modeling to interpret $\delta^{13}\text{C}$ values of syndepositional carbonate spherules (>500 μm) and fine-grained micrite (<63 μm) from a ~1600-year-long sediment record of a hypersaline lake located on the coral atoll of Kiritimati, Republic of Kiribati (1.9°N, 157.4°W). Petrographic, mineralogic, and stable isotope results suggest that both carbonate fractions precipitate *in situ* with minor diagenetic alterations. The $\delta^{13}\text{C}$ values of spherules are high compared to the syndepositional micrite and cannot be explained by mineral differences or external perturbations, suggesting a role for local biological processes. We use geochemical modeling to test the hypothesis that the spherules form in the surface microbial mat during peak diurnal photosynthesis when the $\delta^{13}\text{C}$ value of dissolved inorganic carbon is elevated. In contrast, we hypothesize that the micrite may precipitate more continuously in the water as well as in sub-surface, heterotrophic layers of the microbial mat. Both metagenome and geochemical model results support a critical role for photosynthesis in influencing carbonate $\delta^{13}\text{C}$ values. The down-core spherule–micrite offset in $\delta^{13}\text{C}$ values also aligns with total organic carbon values, suggesting that the difference in the $\delta^{13}\text{C}$ values of spherules and micrite may be a more robust, inorganic indicator of variability in productivity and local biological processes through time than the $\delta^{13}\text{C}$ values of individual carbonate forms.

KEYWORDS

carbonate, microbial mat, stable isotopes, carbon cycle, metagenomics, geochemical modeling

This is an open access article under the terms of the [Creative Commons Attribution-NonCommercial](https://creativecommons.org/licenses/by-nc/4.0/) License, which permits use, distribution and reproduction in any medium, provided the original work is properly cited and is not used for commercial purposes.

© 2022 The Authors. *Geobiology* published by John Wiley & Sons Ltd.

1 | INTRODUCTION

Carbonates from marine and lacustrine environments are key records of past environmental and carbon (C) cycle changes at local, regional, and global scales (Kump & Arthur, 1999; Leng & Marshall, 2004; Talbot & Kelts, 1990). In particular, carbonate stable carbon isotope values ($\delta^{13}\text{C}$) are commonly used as proxies for reconstructing past physiochemical conditions, productivity, organic carbon burial, and biotic/abiotic interactions (e.g., Kump & Arthur, 1999; Newell et al., 2017; Petryshyn et al., 2016; Solari et al., 2010). Additionally, since carbonate precipitation often involves minimal isotopic fractionation from the dissolved inorganic carbon (DIC) pool, and the $\delta^{13}\text{C}$ values of precipitated carbonates are relatively insensitive to temperature changes, carbonate $\delta^{13}\text{C}$ values of stratigraphic units are considered close approximates of the ocean or lake DIC pool (Saltzman & Thomas, 2012 and references therein). However, carbonate $\delta^{13}\text{C}$ values remain challenging to interpret, as multiple processes influence the DIC $\delta^{13}\text{C}$ values that are ultimately recorded by carbonate $\delta^{13}\text{C}$ values. For example, organic matter remineralization (Teranes & Bernasconi, 2005), atmospheric and groundwater sources of DIC (Bade et al., 2004; Patterson & Walter, 1994; Talbot, 1990) and local biological processes (Cohen et al., 2000; Geyman & Maloof, 2019; Leng & Marshall, 2004), have all been shown to affect carbonate $\delta^{13}\text{C}$ values. Furthermore, certain carbonate grains and facies can be influenced by specific microbial and hydrological processes (Andres et al., 2006; Ingalls et al., 2020), resulting in grain-specific $\delta^{13}\text{C}$ values that can be rendered indistinguishable when $\delta^{13}\text{C}$ values are measured on bulk carbonate sediment samples.

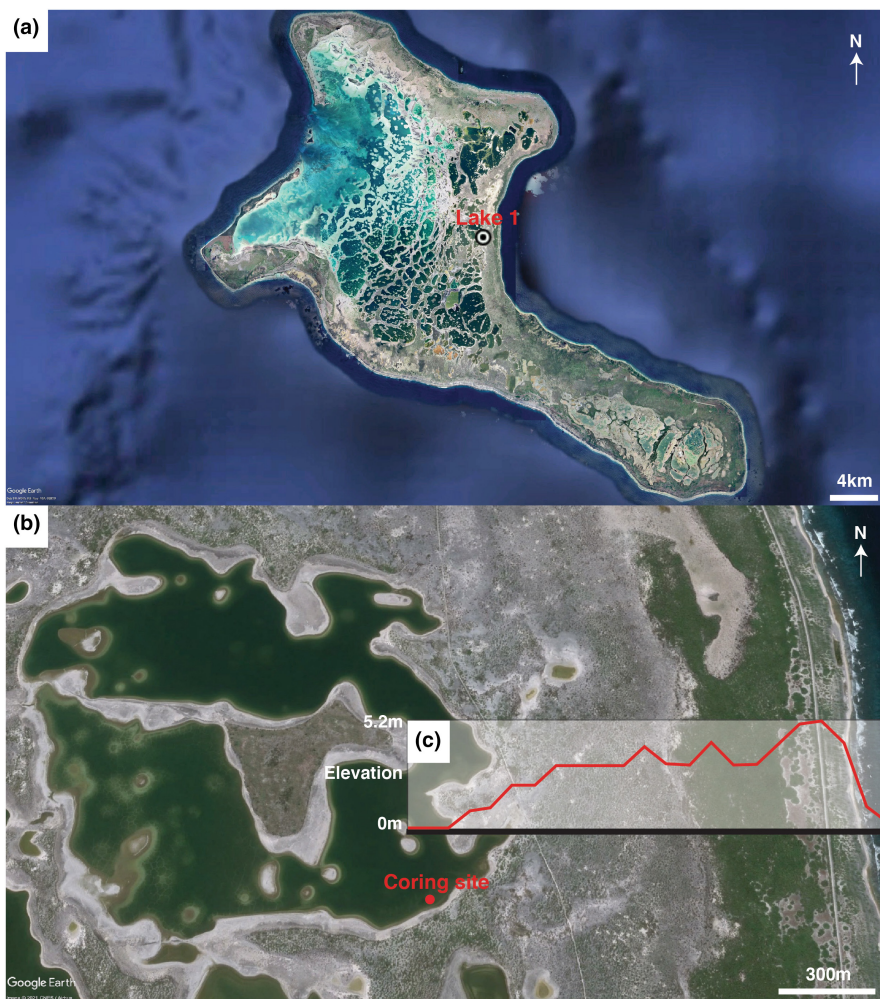
Recently, carbonate facies- and mineral-specific $\delta^{13}\text{C}$ studies of lacustrine and marine sediments have revealed different local and regional impacts on $\delta^{13}\text{C}$ values. For example, in the Great Salt Lake, the $\delta^{13}\text{C}$ values of microbialites, intraclasts, and carbonate mud appear to be impacted by different local processes, such as microbial activity and hydrology, whereas ooid grainstones appear to be more faithful records of time-averaged lake chemistry (Ingalls et al., 2020). Furthermore, the different $\delta^{13}\text{C}$ values of calcite and aragonite in alkaline Lake Van (Turkey) indicate they precipitate in different seasons, with calcite predominantly precipitating during spring under near-freshwater conditions, and aragonite mainly precipitating in summer, when lake water is more evaporated (McCormack et al., 2019). In the Great Bahama Bank, the $\delta^{13}\text{C}$ values of different carbonate facies were found to be impacted by local platform processes and marine and meteoric diagenesis, resulting in the decoupling of carbonate $\delta^{13}\text{C}$ values from open ocean values (Geyman & Maloof, 2021). However, to date, studies that examine the $\delta^{13}\text{C}$ values of carbonate material that are bimodal with respect to microfabric and formation process in the same sedimentary horizons remain rare.

Shallow, near-marine lacustrine environments are ideal places for studying syndepositional carbonates with different microfabric textures and formation processes, since the microbial mats often

present in these environments can provide nuclei or binding sites that favor the growth of carbonate grains larger than sand size (Dupraz et al., 2009), while clay- to silt-size carbonate grains can also be transported, or form locally in the water column, water/sediment interface, or on the surface mat due to supersaturated conditions (Milliman et al., 1993; Morse et al., 2003). Thus, separating coarse- and fine-grained fractions of bulk carbonates and measuring their respective $\delta^{13}\text{C}$ values in these environments may refine interpretations of these values and help identify the processes that drive carbonate formation. The Kiritimati Atoll (Republic of Kiribati, 1.9°N, 157.4°W), one of the Northern Line Islands in the central tropical Pacific (Figure 1a), contains hundreds of brackish to hypersaline carbonate-rich lakes (Saenger et al., 2006) and is an ideal modern analog for restricted lagoonal and near-marine lacustrine carbonate facies (Read, 1985). It is also an ideal location to investigate microbial processes driving carbonate precipitation, as many of the lakes contain actively lithifying microbial mats (Arp et al., 2012; Ionescu et al., 2015; Schmitt et al., 2019; Schneider et al., 2013). Abundant, mm-scale single and aggregated subspherical particles (spherules), which have a morphology similar to ooids, and have also been referred to as ooids (Suarez-Gonzalez & Reitner, 2021), along with predominantly fine-grained carbonates, co-exist in a sediment core retrieved from one of these shallow hypersaline lakes (referred to as Lake 1) in the northeastern interior of the island (Figure 1b, Table S3).

In addition to the more traditional methods of petrography and stable isotope geochemistry, geochemical modeling and metagenomics are methods that can provide quantitative information on the biological processes recorded in carbonate $\delta^{13}\text{C}$ values (Geyman & Maloof, 2019, 2021; Ingalls et al., 2020; Wong et al., 2018). In this study, we use geochemical, petrographic, and molecular microbial information to assess how syndepositional carbonate spherules and micrite in a ~1600-year-long sediment core record C-cycle processes and their temporal variability. We also examine water chemistry data collected from a set of lakes in Kiritimati to support our inferences. We hypothesize that aragonitic spherules form in the surface of microbial mats during peak photosynthesis and thus record different $\delta^{13}\text{C}$ values than the syndepositional micrite, which may form more continuously in the water column, surface mat, and deeper in the mat. To test this hypothesis, we first present the carbonate sedimentology and mineralogy and evaluate the record for evidence of diagenesis. Next, we present and compare the stable carbon and oxygen isotope ratios of paired spherules and micrite from the same depth horizons of the sediment core. We then evaluate the potential drivers of the observed carbonate $\delta^{13}\text{C}$ ($\delta^{13}\text{C}_{\text{carb}}$) values using metagenomics and geochemical modeling results. Finally, we examine the $\delta^{13}\text{C}$ offset of the spherules and micrite throughout the sediment core, along with commonly measured total organic carbon and nitrogen values and their stable isotope ratios. We explain how this $\delta^{13}\text{C}$ offset may be an archive of local biological productivity, and therefore could ultimately be an additional tool to help deconvolve carbon cycle information in the geological record.

FIGURE 1 (a) Image of Kiritimati. The red dot indicates Lake 1 (Adapted from *Google Earth Pro*). (b) Image of Lake 1. The red dot shows the coring site (Adapted from *Google Earth Pro*). The black solid line shows the transect for the elevation profile from Lake 1 to shoreline in (c). White arrows indicate the north direction. (c) Elevation profile as indicated in (b), which is retrieved from *Google Earth Pro*



2 | METHODS

2.1 | Water and sediment sampling

We measured lake temperature ($\pm 0.2^\circ\text{C}$), specific conductivity relative to 25°C ($\mu\text{S}/\text{cm}$), pH (0.01 units), and dissolved oxygen (± 0.02) *in situ* using an YSI Professional Plus multiparameter datasonde in July 2014, July 2017, and June 2019. We calculated salinity in ppt from these data using the Gibbs Sea Water (GSW) Oceanographic Toolbox (McDougall & Barker, 2011). We measured alkalinity in the field using a Hach Company alkalinity test kit. We filtered water samples for cation and anion analysis with 5 and $0.22\ \mu\text{m}$ filters and stored the samples in pre-acidified amber plastic bottles in a dark, refrigerated environment until analysis. We measured major cation concentrations with ICP-OES (Perkin-Elmer, Optima 5300 DV) with a precision of $\pm 2\%$ and major anions with Dionex ICS 3000 gas chromatograph with a precision of $\pm 5\%$. We filtered samples for water isotope analysis ($\delta^{18}\text{O}$ and $\delta^2\text{H}$) and carbon isotope analysis of DIC ($\delta^{13}\text{C}$ of DIC) using 5 and $0.2\ \mu\text{m}$ filters and stored the samples in a 4°C freezer in 30-mL brown HPDE vials without headspace prior to analysis. We used Geochemist's Workbench (Bethke et al., 2020) to

calculate the saturation state (Ω) of carbonate minerals (aragonite and calcite) from measured values of temperature, pH, alkalinity, and ion concentration.

In July 2017, we retrieved a 48-cm core from near the southeastern shore of Lake 1 using an SDI mini-Vibe vibracorer. A green- and red-pigmented, un-lithified microbial mat covered the surface (0–5 cm) of the core (Figure S1). We extruded the core in the field at 2.5 cm intervals (20 sub-samples in total), sampling from the extruded core interior to avoid contamination. We placed pairs of samples in sterile whirlpak bags using sterile spatulas. We treated samples for nucleic acid extraction with RNAlater preservative (Thermo Fisher Scientific), homogenized them, and stored them on ice. Upon return, we stored sediment samples for geochemistry and mineralogy analyses at 4°C in the dark until further analysis, and stored sediment samples for nucleic acid extraction and metagenomics in a -20°C freezer. In the lab, we used 500 and $63\ \mu\text{m}$ sieves to separate the coarse and fine fractions for each sampling depth. We screened and described samples from different sieve pans (>500 , 63, and $<63\ \mu\text{m}$ bases) at $10\times$ – $100\times$ with a dissecting microscope and stored the dry samples in separate vials for subsequent measurement.

2.2 | Petrographic and mineralogy measurements

We obtained thin sections from Wagner Petrographic (Linden, UT) of representative spherule samples from five depths of the 2017 core (2.5, 10, 20, 30, and 40.2 cm), sampling 10–15 carbonate spherules at each depth. We first assessed sample texture, preservation, and mineralogy using transmitted light (TL) microscopy at the Carl R. Woese Institute of Genomic Biology at the University of Illinois Urbana-Champaign (UIUC). We examined spherules with distinctive features (e.g., organic matter (OM) nuclei or laminae, post-depositional alterations, and embedded microfossils) with a Tescan Scanning Electron Microscope (SEM) using environmental mode (Univac 20 Pa) in the UIUC Department of Geology. We generated elemental maps (C, O, Na, Mg, Si, P, S, Cl, Ca, and Sr) for selected spherules using an energy-dispersive spectrometer (EDS) attached to the SEM. We viewed another set of spherules and associated matrix on glass slides affixed with carbon tape under SEM to obtain information about the topography and mineral-OM relationships within the matrix.

To provide mineralogical context supporting the petrographic results, we collected X-ray diffraction (XRD) data on representative spherules and matrix samples from the Lake 1 core. To remove soluble salts, we centrifuged the wet samples of spherules (>500 μm) and matrix (<63 μm) in Milli-Q water for 10 min at 2800 RPMs, and repeated three times. We then transferred samples to Petri dishes, where we removed organics with 30% hydrogen peroxide. We then air-dried samples in the fume hood and ground them into powders with mortar and pestle. We ran pulverized spherule and matrix samples on a Siemens-Bruker D5000 at the Frederick Seitz Materials Research Laboratory at the UIUC with the following settings: incident angle of 5°–90°, an increment of 0.02, and a scan speed of 1°/min. We analyzed results in the Jade XRD software to obtain mineral identification and abundances.

2.3 | Chronology

Our chronology of Lake 1 is built upon three acid–base–acid pre-treated radiocarbon dates on organic matter (Chen et al., 2020). We created an age–depth model using Bacon 2.2 (Blaauw & Christen, 2011), after correcting for a surface radiocarbon reservoir effect of 350 years and using INTCAL13 (Reimer et al., 2013). Modeled ages are in calendar years.

2.4 | Stable isotope measurements

Using a mortar and pestle, we crushed the rinsed spherules (>500 μm) and matrix (<63 μm) at each sampling depth. We measured the $\delta^{13}\text{C}$ and $\delta^{18}\text{O}$ values of these prepared carbonates and the $\delta^{13}\text{C}$ of water DIC on a Kiel III automated carbonate preparation device coupled to a Finnigan MAT 252 in the Illinois State Geological Survey (ISGS) Stable Isotope Laboratory. We added silver foil to each run

to remove potential sulfate contamination. After completely removing inorganic carbonate with 10% HCl, we measured organic carbon, along with total carbon and total nitrogen percentages of the organic matrix (TOC, $\delta^{13}\text{C}_{\text{org}}$, and TN), on an EA-IRMS (CE Instruments NC 2500 elemental analyzer in series with a ConFlo IV universal interface coupled to a Delta V Advantage Isotope Ratio Mass Spectrometer) housed at the Illinois State Geological Survey (ISGS) (Chen et al., 2020). Precision is $\pm 0.02\text{‰}$ for $\delta^{13}\text{C}_{\text{org}}$ (VPDB), $\pm 0.02\text{‰}$ for $\delta^{13}\text{C}_{\text{carb}}$ (VPDB), $\pm 0.07\text{‰}$ for $\delta^{18}\text{O}_{\text{carb}}$ (VPDB), and $\pm 0.03\text{‰}$ for $\delta^{13}\text{C}_{\text{DIC}}$ (VPDB). We measured the water $\delta^{18}\text{O}$ and $\delta^2\text{H}$ on a Picarro L2130-i cavity ringdown isotopic analyzer in the UIUC Department of Geology. The average precision is $\pm 0.1\text{‰}$ for $\delta^{18}\text{O}$ (VSMOW) and $\pm 0.8\text{‰}$ for $\delta^2\text{H}$ (VSMOW).

2.5 | Sequencing, taxonomic, and functional genes analyses

For the 2017 sediment core, we extracted DNA of representative sediment subsamples (0.5 g) from 17 individual sample depths, with duplicates, using a modified protocol for extraction of DNA and RNA from soil using phenol–chloroform methods. Protocol details with explicit modifications and related references are in the supplemental materials. The quality and quantity of extracted DNA were determined by agarose gel electrophoresis and fluorometry (Qubit 4.0). We sequenced five metagenomes (MET-1: 0–5 cm, MET-2: 5–22.5 cm, MET-3: 22.5–34.2 cm, MET-4: 34.2–38 cm, and MET-5: 38–40.2 cm) in the UI Carver Biotechnology Center using the Illumina HiSeq 4000 platform (Chen et al., 2020). For each sequenced library, we obtained the taxonomic annotations from the DIAMOND-MEGAN pipeline (Buchfink et al., 2014; Huson et al., 2016) and the functional gene annotations from metagenomes deposited to JGI-Integrated Microbial Genomes and Microbiomes (JGI-IMG) (Chen et al., 2019). Detailed sequence analysis procedures can be found in Chen et al. (2020).

For each metagenome, we used the annotations to extract the cited taxa and signature functional genes associated with microbial activities that can directly or indirectly induce carbonate precipitation (Berg et al., 2010; Zhu & Dittrich, 2016; and references therein) (Table 2). We used the R package “phyloseq” (McMurdie & Holmes, 2013) to quality filter, normalize, and visualize the clustered operational taxonomic units (OTUs) from the DIAMOND-MEGAN pipeline. We normalized the relative abundance of each functional gene from KEGG annotations using the *rpoB* gene (the beta subunit of bacterial RNA polymerase) to obtain the relative abundance of different functional genes related to carbonate precipitation in each metagenome (Orellana et al., 2018). Additionally, we used Functional Annotation of Prokaryotic Taxa (FAPROTAX) to predict established metabolic functions from the valid 16S rRNA sequences obtained from MEGAN-DIAMOND pipeline based on the characterized strains obtained via OTU tables with putative functional tables in the FAPROTAX database (Louca et al., 2016). Finally, we visualized the relative abundances of genes and metabolisms using a heatmap

function from the R package “NMF” to observe the distributions of critical enzymes potentially involved in carbonate precipitation at different depths in the sediment core (Gaujoux & Seoighe, 2010).

2.6 | Geochemical modeling

To simulate carbonate $\delta^{13}\text{C}$ values in Lake 1, we used a simple mass balance model of the diurnal carbon engine, modified from Geyman and Maloof (2019) (Figure 2). This model, which was developed to explain the anomalously high $\delta^{13}\text{C}$ values of modern carbonates on the Bahama Bank, shows how the daily cycle of photosynthesis and respiration can lead to the decoupling of global seawater $\delta^{13}\text{C}$ values and shallow water carbonate $\delta^{13}\text{C}$ values.

The primary forcing of the model is the daily organic CO_2 flux (F_{org}) from photosynthetic and aerobic respiration, resulting in the transfer of carbon between the inorganic and organic reservoirs. The diurnal periodicity of F_{org} is approximated from several shallow marine settings from high-resolution (~hourly) DIC/TA/pH/ $p\text{CO}_2$ data (Geyman & Maloof, 2019). The amplitude of the F_{org} (κ_p) is estimated from a Deffeyes diagram by calculating the diurnal DIC change induced by photosynthesis (Geyman & Maloof, 2019). This value can range from 19 $\mu\text{mol}/\text{kg}$ in the open ocean to ~600 $\mu\text{mol}/\text{kg}$ in some shallow marine settings. Therefore, we used a range of κ_p (from 200 to 600 $\mu\text{mol}/\text{kg}$) to simulate different amplitudes of F_{org} in our system. For sensitivity tests, we used $\kappa_p = 247 \mu\text{mol}/\text{kg}$, which is the median photosynthetic forcing in the Geyman and Maloof (2019) compilation, as the default setting. The two other significant carbon fluxes in the model are carbonate precipitation/dissolution (F_{carb}) and gas exchange (F_{gas}). We used parameterizations for F_{carb} and F_{gas} that are widely used in the literature (Table S1). We divided each day into time steps of 5 min. In each timestep, we use the lake water DIC

and TA to compute the lake water $p\text{CO}_2$ and saturation state of aragonite (Ω_{Ar}) and calcite (Ω_{Ca}) in CO2SYS (Lewis & Wallace, 1998). We then used $p\text{CO}_2$ and Ω to calculate F_{carb} and F_{gas} (Table S1). Next, we apply the forcings F_{org} , as well as the computed F_{carb} and F_{gas} fluxes, to track the evolving lake DIC and TA based on the stoichiometry of carbonate precipitation, photosynthesis, and air–sea CO_2 gas exchange (Geyman & Maloof, 2019). The detailed equations and the descriptions of all model variables are listed in Table S2 and Figure 2.

The input variables and the fractionation factors (ϵ) for carbon transfer between different reservoirs (atmosphere, organic carbon, and lake DIC) are listed in Table S2 and Figure 2. We estimated the fractionation factor between the DIC pool and organic matter (ϵ_p) from paired $\delta^{13}\text{C}_{\text{org}}$ and $\delta^{13}\text{C}_{\text{carb}}$ measurements for each sampling depth (see Supplemental Materials for details). We computed a median value of $\epsilon_p = -10\%$, which is comparable to other hypersaline microbial mats (Houghton et al., 2014; Kelley et al., 2006). We used literature values for the fractionation factors between carbonate minerals and the DIC pool (ϵ_{arag} , $\epsilon_{\text{calcite}}$), as well as between the DIC pool and the atmosphere ($\epsilon_{\text{air-lake}}$, $\epsilon_{\text{lake-air}}$) (Table S2).

To understand how mineral composition influences carbonate $\delta^{13}\text{C}$ values, we tracked the $\delta^{13}\text{C}$ values of calcite and aragonite over 24 h of precipitation in the model. Additionally, we conducted a series of sensitivity tests (Table S2) to determine which variables may drive the high $\delta^{13}\text{C}$ values of spherules and the magnitude of the $\delta^{13}\text{C}$ offset between co-occurring spherule and micrite $\delta^{13}\text{C}$ values. Input parameters that can significantly shift due to environmental changes were included in the sensitivity tests (Table S2). For the sensitivity tests, we changed one parameter of interest at a time and chose the range of model inputs from either (1) end members of field observations or (2) calculations based on our field measurements. To evaluate the impact of different diurnal patterns of precipitation on the simulated carbonate $\delta^{13}\text{C}$ values, we also applied different precipitation

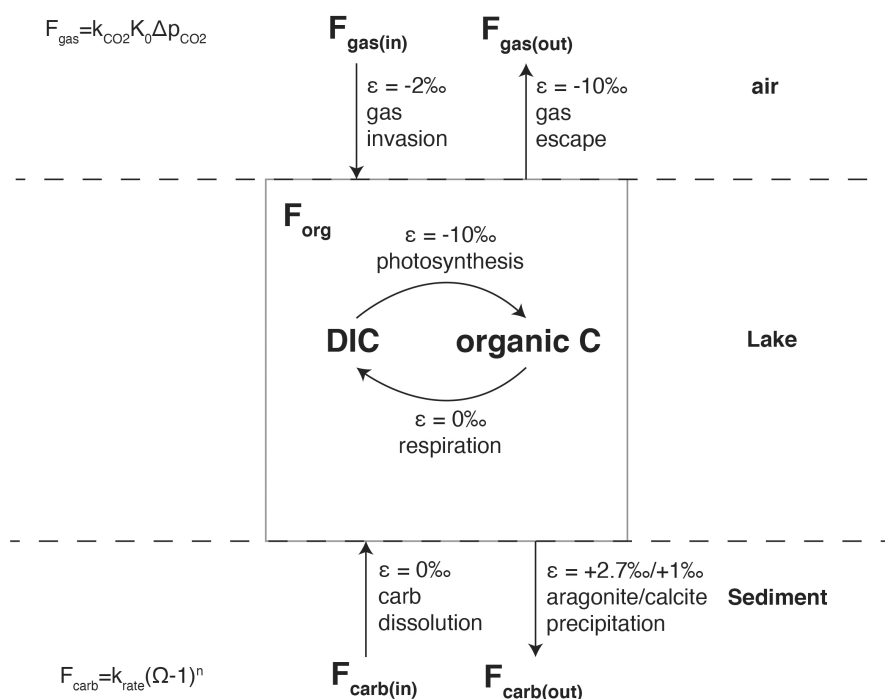


FIGURE 2 A numerical mass balance model modified from Geyman and Maloof (2019) tracks the $\delta^{13}\text{C}$ composition and mass fluxes of carbon transferred through air–lake gas exchange, carbonate precipitation/dissolution, and photosynthesis/respiration. See Tables S1 and S2 for more details about the parameters used in the equations to calculate each flux

periods, varying from 2 to 24 h around peak photosynthesis. Peak diurnal photosynthesis was defined as 15:00, the time with the highest instantaneous $\delta^{13}\text{C}_{\text{DIC}}$ values when running the model for a 24-h cycle (Figure S1). This timing of peak photosynthesis is supported by diurnal $\delta^{13}\text{C}_{\text{DIC}}$ variability observed in shallow reefs, showing the highest $\delta^{13}\text{C}_{\text{DIC}}$ values around 15:00 (Geyman & Maloof, 2019; Richardson et al., 2017). We calculated the weighted $\delta^{13}\text{C}$ average

for each precipitation period ($\delta^{13}\text{C}_{\text{weighted}} = \frac{\sum F_{\text{carb}} \times \delta^{13}\text{C}}{\sum F_{\text{carb}}}$). We ran all models for 50 days (20,000 timesteps) to reach a stable value for the weighted $\delta^{13}\text{C}$ average. We recorded the weighted $\delta^{13}\text{C}$ average for different precipitation hours around peak diurnal photosynthesis (2–24 h) for each sensitivity test and computed the $\delta^{13}\text{C}$ offset between each period and the daily average $\delta^{13}\text{C}$ value. We use contour maps to illustrate the $\delta^{13}\text{C}_{\text{carb}}$ and $\delta^{13}\text{C}$ offsets for different sensitivity tests (see Supplemental Materials for code).

Finally, we make alternative calculations of the $\delta^{13}\text{C}_{\text{carb}}$ and $\delta^{13}\text{C}$ offsets using pCO_2 and saturation indices calculated with the PHREEQC program (Parkhurst & Appelo, 2013). The comparison of these two carbonate system modeling methods (PHREEQC and CO2SYS) showed good agreement for most physiochemical parameters. However, at high salinity, the PHREEQC modeling method likely provides more accurate carbonate system parameters, since CO2SYS does not contain a dataset for high salinity conditions (see Appendix S3).

3 | RESULTS

3.1 | Water chemistry

The surface water chemistry of Lake 1 varied substantially in different years, most notably in salinity, with values ranging from mesosaline (44.9 ppt, 2017) to hypersaline (147.3 ppt, 2014) (Table 1). The alkalinity of Lake 1 also varied from 4.42 meq/L (2014) to 1.32 meq/L (2019). The DO values in the lake varied from 61.6% (2014) to 90.5% (2019), and all three measurements fall within the hyperoxic range due to photosynthetic activity. As DO was not measured at the same time every day and also has significant diurnal variations (Geyman & Maloof, 2019), these values are not used as indicators of photosynthetic rates. The pH values (7.81 to 8.17) and water temperatures (29.7–31.9°C) for Lake 1 were relatively stable over measurement periods.

The 2014 $\delta^{18}\text{O}$ values of Kiritimati lake waters, taken from a suite of lakes, range from -0.77‰ (Lake 24) to 4.94‰ (Lake 27). The $\delta^2\text{H}$ values range from -6.59‰ (Lake 24) to 24.92‰ (Lake 26). The $\delta^{18}\text{O}$ values of the 2019 Kiritimati lake water range from 0.51‰ (Lake 150) to 2.40‰ (Lake F7). The $\delta^2\text{H}$ values range from 2.24‰ (Lake 18) to 13.68‰ (Lake F7). The $\delta^{13}\text{C}$ values of the 2019 Kiritimati lake water DIC range from -13.47‰ (Lake F6) to 1.73‰ (Lake 15), with a median value of -2.11‰ (Table S4). The measured $\delta^{18}\text{O}$, $\delta^2\text{H}$, and $\delta^{13}\text{C}_{\text{DIC}}$ values of Lake 1 in 2019 (sampled at 9:36 AM) are 1.47‰ , 6.51‰ , and -4.74‰ , respectively.

TABLE 1 Physical and chemical properties of Lake 1 on July 2014, June 2017, and June 2019

Sample ID	K14-01	K17-01	K19-01
$\delta^{18}\text{O}$ (‰, VSMOW)	1.81	2.66	1.47
$\delta^2\text{H}$ (‰, VSMOW)	3.75	12.31	6.51
Temperature (°C)	31.2	31.9	29.7
DO (%)	61.6	84.9	90.5
Conductivity ($\mu\text{S}/\text{cm}$)	176384	75141	108305
Salinity (ppt)	147	44	72
pH	8.04	7.81	8.17
Alkalinity (meq/L)	4.4	2.20	1.32
Ca (mmol/kgw)	1241	1613	2772
Mg (mmol/kgw)	6170	1917	4059
Na (mmol/kgw)	50890	17262	37388
K (mmol/kgw)	1879	663	7689
Sr (mmol/kgw)	31.68	N.D.	28.46
Si (mmol/kgw)	1.87	N.D.	N.D.
B ($\mu\text{mol}/\text{kgw}$)	24432	N.D.	N.D.
Mg/Ca	4.97	1.19	1.46
Cl (mmol/kgw)	N.D.	25532	33000
SO_4 (mmol/kgw)	N.D.	5844	8700
Saturation State (Ω) Aragonite	10.23	4.68	6.03
Saturation State (Ω) Calcite	14.79	6.92	8.71

ND, not detected.

3.2 | Sedimentary chronology, sedimentology, and mineralogy results

The interpolated bottom age of the core is 1590 ± 20 cal yr before present (BP), and the age at the bottom (5 cm) of the modern microbial mat is 130 ± 15 cal yr BP. The inferred sedimentation rate is 0.02 cm/yr from 2.5 to 22.5 cm and 0.04 cm/yr from 22.5 to 48 cm (Chen et al., 2020). A detailed description of the core sediment can be found in the previous literature (Chen et al., 2020). The core top consists of a green- and red-pigmented, unlithified microbial mat (~5 cm thick). Brown, thin-bedded carbonate aggregates and spherules (0.5–1 mm) are abundant. The sediments beneath the surface microbial mat consist of uncemented carbonate sediments of varying grain sizes (μm to mm), along with dispersive red- to brown-pigmented OM. There is abundant red-brown, thin-bedded micritic calcite and aragonite in the 5–10 cm section of the sediment core, along with carbonate spherules (0.5–2 mm) and red-pigmented OM. Between 10 and 34.3 cm in depth, the relative abundances of dark-brown micrite decrease substantially, whereas the abundance of coarse-grained spherules and plate-like carbonate fragments (0.5 and 2 mm in diameter) increases. From 34.3 to 40.2 cm, the sediment is dominated by brown, thin-bedded micritic carbonate with some sand-size carbonate particles, along with gastropods, bivalve

and coral fragments, and a dark red–brown laminated microbial mat (located at 40.2 cm, referred to as buried mat). Underneath 40.2 cm to the bottom (48 cm) of the core, there is a sharp change to white, massive carbonate silt with knobby carbonate aggregates and gastropods, bivalves, and coral fragments. The interpretations and analyses that follow focus on sediments above this transition boundary.

The primary, inorganic coarse-grained carbonates (>500 μm) in the studied region of Lake 1 sediment core (0–40.2 cm) are single or aggregated subspherical particles with grain sizes ranging from 0.5 to 2 mm (Figure 3a,b), referred to as “spherulites” or “spherules” in the previous Kiritimati literature given their spherical shape (Arp et al., 2012; Schmitt et al., 2019; Schneider et al., 2013), and more recently considered as ooids (Suarez-Gonzalez & Reitner, 2021). Since our primary interest is in the C-cycle information encoded in different components of the sedimentary column, we do not take a stance on the semantic argument of whether these subspherical particles should be referred to as ooids, and instead use the broader term “spherules”. As shown in Figure 3a,b, the surfaces of the spherules are often irregular and pitted, similar to those found in other Kiritimati lakes (Suarez-Gonzalez & Reitner, 2021). The petrographic images of spherules show signs of diagenesis, including borings, dissolution (pitting), isopachous crusts of fibrous aragonite cement, and recrystallization (Figure S4), suggesting that they have undergone some alteration. Spherules are found in all depths of the sediment core (from 0 to 40.2 cm, Table S3), and are also found cemented together, forming irregular aggregates, similar to those found in other Kiritimati lakes (Schmitt et al., 2019; Suarez-Gonzalez & Reitner, 2021). The number of individual spherules and aggregated spherules does not differ substantially across the 40.2-cm core (Table S3). The spherules often consist of a nucleus and a cortex (Figures 3c–e), but some spherules without a clear nucleus are also found in the sediment (Figure 3f). The nuclei are always irregular micritic aggregates, potentially including organic matter, such as extracellular polymeric substances (EPS). The cortices of the particles have radial fibrous structures composed of aragonite minerals (Figure 3c, e), and some of the cortices also include internal laminations (Figure 3d). Several spherules have morphological features indicative of ooids (Suarez-Gonzalez & Reitner, 2021), such as radial fibrous and micritic laminae forming around a central nucleus (Figure 3d). Spherules with and without internal laminations are both consistently present across the sediment core, and there is no significant difference between the ratios of these two types of spherules. XRD results of powdered spherule samples show that they are aragonite, and elemental abundance results from EDS-XRF indicate spherules are predominantly Ca rich, with minimal Mg hotspots (Figure S5B–C, E–F). Skeletal grains (e.g., gastropods, fossil coral fragments, and bivalve shells) are also found in the coarse-grained carbonate fraction but are much less abundant and only found in 34.2 to 48 cm of the sediment core, adjacent to the lagoon transition zone at 48 cm.

Primary fine-grained carbonates (<63 μm) are mainly composed of needle-like aragonite and calcite crystal aggregates. SEM imagery of the matrix shows evidence of initial microcrystalline carbonate

crystal aggregates (from <1 to 50 μm) associated with EPS, as well as silt-sized aragonite crystal aggregates (Figure 3g,h). XRD results of the fine-grained samples indicate a mixture of aragonite and calcite (aragonite: $86.2 \pm 5.0\%$; calcite: $13.8 \pm 5.0\%$, Table S3).

3.3 | Stable isotope results

$\delta^{13}\text{C}_{\text{org}}$ values decrease from 0 to 22.5 cm (from -14.25% to -18.26%) and increase from 22.5 to 40.2 cm (from -18.26% to -10.53%). Total organic carbon (TOC) and total nitrogen (TN) are highest in the mat regions (0–5 cm and 38–40.2 cm) and are relatively lower in the middle part of the core (Figure 4). Carbon and oxygen stable isotope values of spherules ($\delta^{13}\text{C}_{\text{sp}}$, $\delta^{18}\text{O}_{\text{sp}}$) vary from 5.31% to 8.11% and -0.39% to 0.42% , respectively. $\delta^{13}\text{C}$ and $\delta^{18}\text{O}$ values of the micrite ($\delta^{13}\text{C}_{\text{m}}$, $\delta^{18}\text{O}_{\text{m}}$) from the sediment core range from 1.41% to 5.77% and -0.67% to 0.29% , respectively. Both spherules and micrite show statistically significant ($r = 0.60$ and 0.75 , $N = 17$, $P < 0.05$ and $P < 0.001$, respectively) positive covariations of $\delta^{13}\text{C}$ and $\delta^{18}\text{O}$ values (Figure 5a). The $\delta^{13}\text{C}_{\text{sp}}$ and $\delta^{18}\text{O}_{\text{sp}}$ values are significantly higher than the $\delta^{13}\text{C}_{\text{m}}$ and $\delta^{18}\text{O}_{\text{m}}$ from the same sampling depth (two-tailed paired t-test, $p < 0.0001$ and $p < 0.001$, respectively).

3.4 | Taxonomic and functional gene results

Microbial taxa known to influence carbonate precipitation (Table 2) comprise 20.7% of the total microbial community for the surface mat (MET-1), which is dominated by bacterial oxygenic phototrophs (phylum Cyanobacteria, 14.5%) and specifically identified anoxygenic phototrophs within the phyla Acidobacteria, Chlorobi, Gemmatimonadetes, and Proteobacteria (4.7%) (Figure 6a). Below the surface mat (MET-2, MET-3, MET-4, and MET-5), the relative abundance of microbial taxa that are involved in carbonate precipitation declines to less than 5% of the total microbial community with more archaeal methanogens (phylum Euryarchaeota) and methanotrophs (phylum Crenarchaeota, related to anaerobic methane oxidation) compared to the surface mat region. On the other hand, the relative abundance of sulfate-reducing bacteria (mainly from class Desulfobacterota, formerly Deltaproteobacteria) stays relatively stable ($1.0 \pm 0.2\%$) across the core.

Functional gene annotations show that genes related to electron transfer of photosynthesis (*psbA/D*, *psaA/B*) along with genes (*rbcl*, *prkB*, *aclA*, *mch*, and *mcl*) that encode key enzymes for carbon fixation pathways (Calvin cycle, reductive TCA, and 3-hydroxypropionate bicycle) used by phototrophs (Wong et al., 2018) are most abundant in the surface mat (Figure 6b). Additionally, functional genes related to sulfate reduction (*cysNC*, *cysD*, *dsrB*, and *aprA*), ammonification (*echA*), and carbonic anhydrase (*cynT*) are also dominant in this region. Functional genes of carbon fixation pathways used by anaerobic microbes (*cooS*, *coxS*, *cdhA*, *acsB*, and *abfD*) dominate in deeper sediments, and most

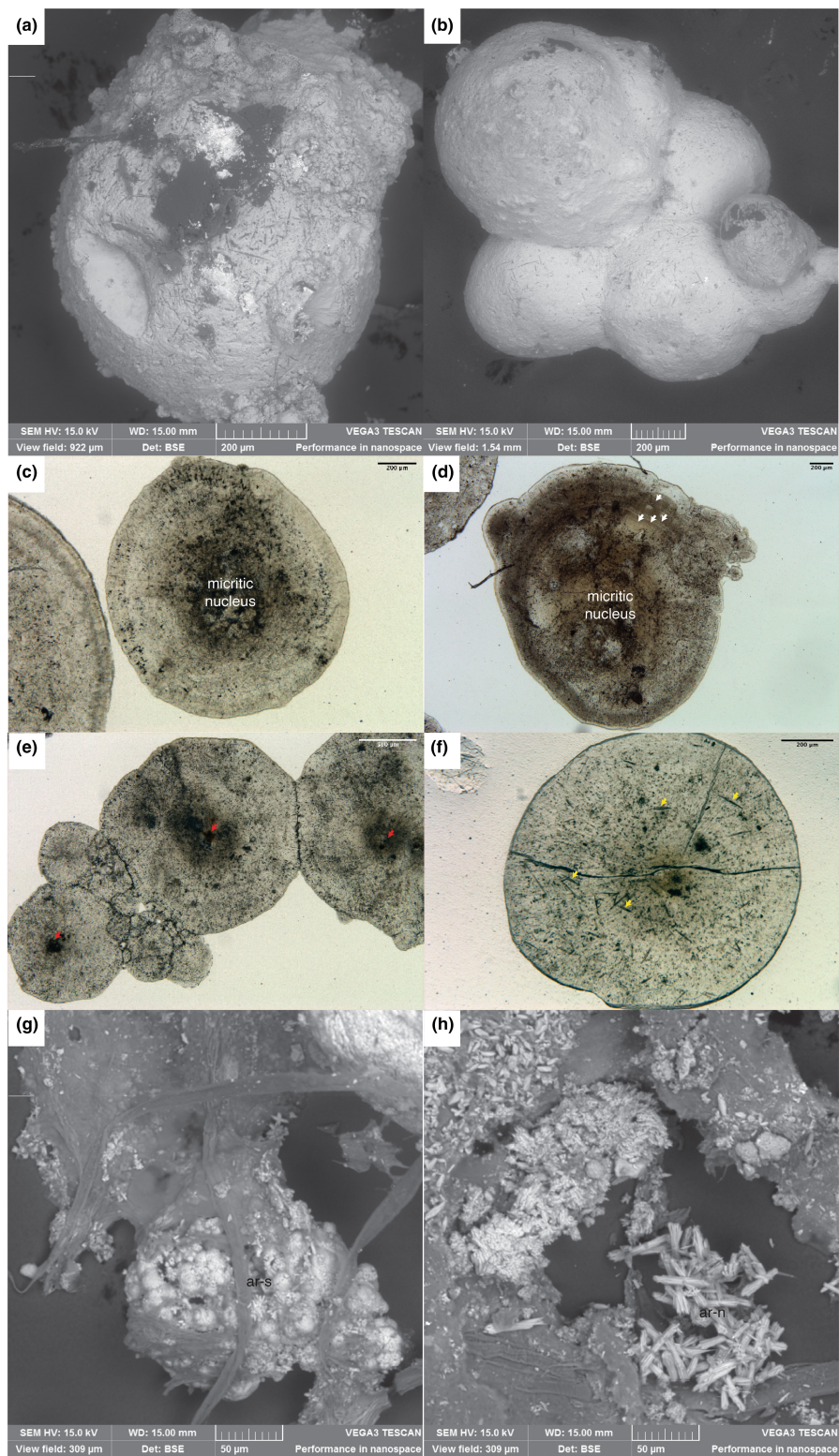


FIGURE 3 Transmitted light and SEM images of typical coarse- and fine-grained carbonates in the Lake 1 sediment core. (a) SEM image of an individual spherule (2.5–5 cm). (b) SEM image of a spherule aggregate (20–22.5 cm). (c) Transmitted light photomicrograph of an individual spherule with a micritic nucleus potentially including OM (2.5–5 cm) and radial fibrous textures, but without strong concentric laminae. (d) Transmitted light photomicrograph of an individual spherule with nucleus (7.5–10 cm), radial fibrous laminae, and micritic laminae (white arrows). Arrows indicate locations of micritic laminae. (e) Transmitted light photomicrograph of spherule aggregates (20–22.5 cm) with a micritic nucleus potentially including OM (red arrows) and radial fibrous laminae. (f) Transmitted light photomicrograph of an individual spherule without an apparent nucleus (2.5–5 cm). Noted that diatoms (yellow arrows) are also trapped within the spherules due to the rapid carbonate precipitation. (g) Initial spherule-like aragonite matrix, showing association with EPS filaments (ar-s, 7.5–10 cm). (h) Needle-like structure of aragonite matrix (ar-n, 7.5–10 cm). Scale bars as indicated in the figures

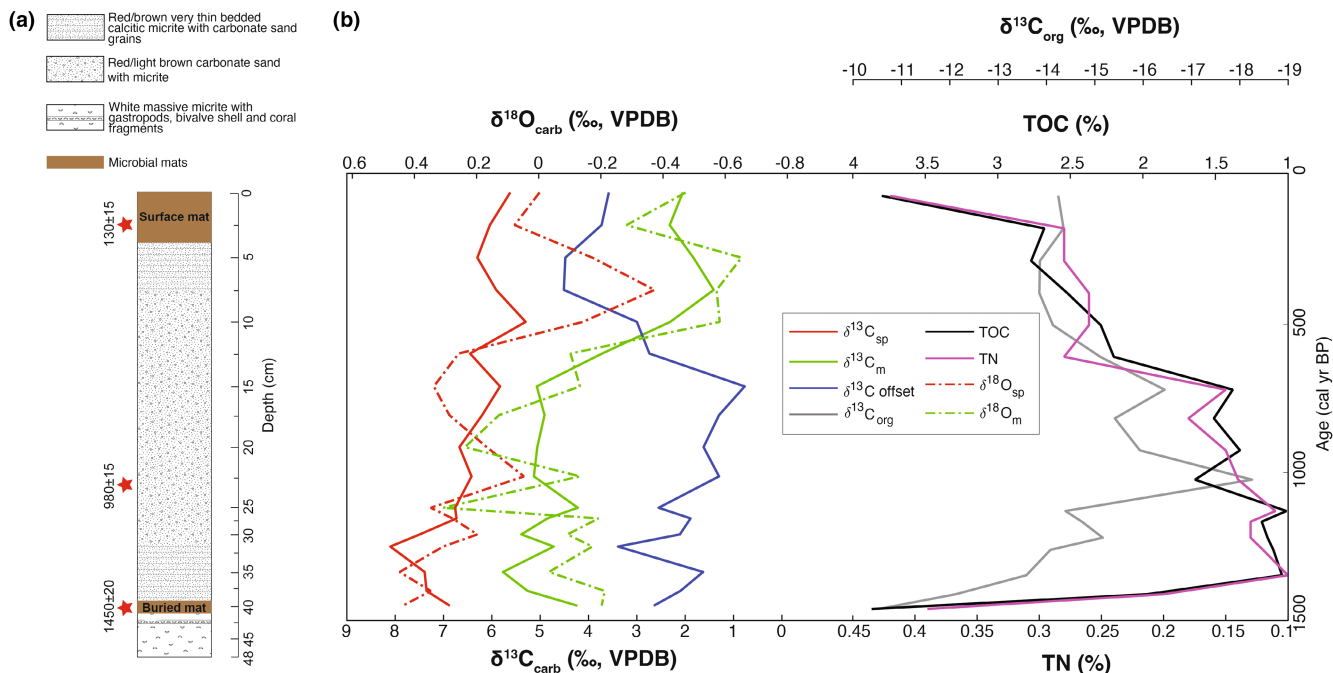


FIGURE 4 (a) Kiritimati Lake 1 core lithology description. Stars indicated calibrated radiocarbon ages (in cal yr BP). (b) Kiritimati Lake 1 spherule $\delta^{13}\text{C}$ values (VPDB, red solid line), micrite $\delta^{13}\text{C}$ values (VPDB, green solid line), $\delta^{13}\text{C}$ offset (VPDB, blue solid line), bulk OM $\delta^{13}\text{C}_{\text{org}}$ (VPDB, gray solid line), percent total organic carbon (black solid line), percent total nitrogen (pink solid line), spherule $\delta^{18}\text{O}$ values (VPDB, red dashed line), and micrite $\delta^{18}\text{O}$ values (VPDB, green dashed line) from 1500 cal yr BP to present

other genes are much less abundant in the deeper sediments. Functional genes from other pathways (e.g., denitrification, methanogenesis, ureolysis, and anaerobic methane oxidation) that can trigger carbonate precipitation directly or indirectly have much lower relative abundance than the functional genes mentioned above (Figure 6b).

3.5 | Geochemical modeling

We simulate the diurnal cycle of $\delta^{13}\text{C}_{\text{DIC}}$ to assess what environmental conditions can help to explain our down-core and grain-specific variability in $\delta^{13}\text{C}$ (Figures 3 and 4). Sensitivity tests indicate that variations in temperature, salinity, wind speed, atmosphere CO_2 pressure, and carbonate precipitation rate only lead to minor changes ($<1\%$) in simulated carbonate $\delta^{13}\text{C}$ values (Figure S6). However, changes in the amplitude of F_{org} (κ_p), the fractionation factor of photosynthesis (ϵ_p), salinity, and the initial $\delta^{13}\text{C}_{\text{DIC}}$ more substantially alter $\delta^{13}\text{C}_{\text{carb}}$ values (Figure 7). Varying κ_p between 200 and 600 $\mu\text{mol}/\text{kg}$ can increase simulated $\delta^{13}\text{C}_{\text{carb}}$ by 2.7‰ (Figure 7a), while changes in ϵ_p from -14.7% to -7.4% drive a $\sim 1.5\%$ shift in simulated $\delta^{13}\text{C}_{\text{carb}}$ (Figure 7c), depending on the duration of carbonate precipitation each day. In addition, the change in initial $\delta^{13}\text{C}_{\text{DIC}}$ from -14% to 6% can lead to a $\sim 20\%$ change in simulated $\delta^{13}\text{C}_{\text{carb}}$ values (Figure 7e), and a change in salinity from 40 to 90 ppt can lead to a $\sim 2\%$ change in simulated $\delta^{13}\text{C}_{\text{carb}}$ values (Figure 7g). As for parameters that can lead to

changes in the $\delta^{13}\text{C}$ offset between the spherules and micrite, only κ_p and the duration of precipitation can lead to substantial changes in the simulated $\delta^{13}\text{C}$ offset (1.2‰) (Figure 7b). Changes to the initial $\delta^{13}\text{C}_{\text{DIC}}$, salinity, and ϵ_p only cause changes in the simulated $\delta^{13}\text{C}$ offset of $<0.6\%$ (Figure 7d, f, h). The different mineral composition (aragonite vs. calcite) of spherules and micrite can lead to a maximum of 0.5‰ daily difference in simulated $\delta^{13}\text{C}_m$ and $\delta^{13}\text{C}_{sp}$ values (Table S6).

4 | DISCUSSION

4.1 | Evaluating carbonates in Lake 1: sources and diagenesis

The $\delta^{13}\text{C}$ and $\delta^{18}\text{O}$ values of bulk carbonates in lacustrine and marine systems have been widely used to interpret local, regional, and global environmental conditions (e.g., Kelts & Talbot, 1990; Kump & Arthur, 1999; Leng & Marshall, 2004). However, transport and diagenesis can complicate these isotope-based paleoenvironmental reconstructions. For example, the stable isotope values of detrital carbonates formed in other systems and transported to a lake or ocean do not represent *in situ* water chemistry (Gierlowski-Kordesch, 2010). Additionally, diagenetic alterations such as secondary mineralization, dissolution, and reprecipitation can alter primary stable isotope values (Higgins et al., 2018; McCormack et al., 2018; Newell et al., 2017; Talbot & Kelts, 1990). Therefore, in the following

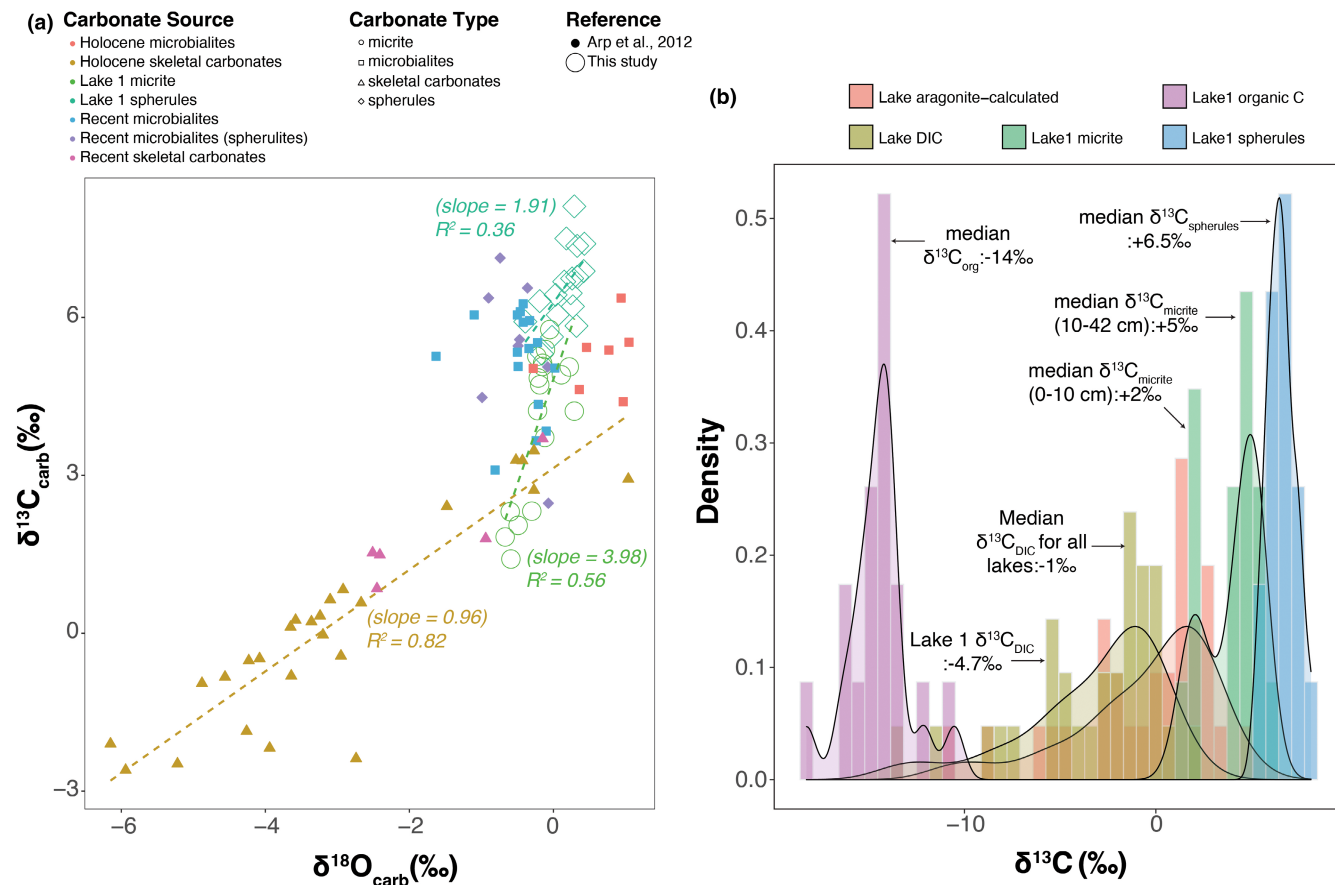


FIGURE 5 (a) Carbon ($\delta^{13}\text{C}_{\text{carb}}$) and oxygen ($\delta^{18}\text{O}_{\text{carb}}$) stable isotope ratios of Kiritimati microbialite (aragonite), skeletal carbonates (aragonite), spherules (aragonite), and micrite (aragonite and calcite) from this study and Arp et al. (2012). The slopes and R^2 -values are shown for trend lines. For carbonates from Arp et al. (2012), the term “Holocene” refers to carbonates collected from the lithified sediments and the term “Recent” refers to carbonates collected from the unlithified sediments. (b) Histogram of the $\delta^{13}\text{C}$ values of organic matter and sediments (micrite and spherules) in Lake 1, the $\delta^{13}\text{C}$ of lake water DIC, and the calculated (predicted) abiotic aragonite $\delta^{13}\text{C}$ value based on lake water DIC and a fractionation factor of +2.7‰ (Romanek et al., 1992)

section, we (1) evaluate the probable sources of the carbonate (*in situ* vs. transported), and (2) discuss evidence for potential diagenetic alteration.

The sources of fine-grained carbonates (i.e., micrite, also referred to as carbonate mud) have long been debated. Carbonate mud has been hypothesized to (1) precipitate directly from the water column (e.g., Milliman et al., 1993), (2) form as the result of the disintegration of calcifying green algae (e.g., Lowenstam & Epstein, 1957), (3) represent the abraded product of carbonate ooids (Trower et al., 2019) or shells (Gischler et al., 2013), or (4) precipitate in relation to the EPS matrix of microbial mat (e.g., Arp et al., 2012). Carbonate mud can also be transported in currents, floods, and storms in marine settings, which can result in mud layers carrying $\delta^{13}\text{C}$ signatures from distant parts of the carbonate system (Geyman & Maloof, 2021). However, the relatively high elevation (maximum ~5.2 m) of the land between Lake 1 and the marine beach 1.3 km to the east (Figure 1c) suggests that the micrite sampled from Lake 1 is unlikely to have been transported in such a manner.

At our study site, the calculated saturation state values indicate that the lake water is consistently supersaturated with respect to

calcite and aragonite (Table 1), so the Lake 1 micrite could directly precipitate from the water column. Based on the data we have gathered so far, there is no direct evidence either supporting or excluding this possibility. On the other hand, the $\delta^{13}\text{C}$ offset between Lake 1 micrite (median $\delta^{13}\text{C}_m = -4.72\text{‰}$) and spherules (median $\delta^{13}\text{C}_{sp} = 6.46\text{‰}$, Figure 5b) suggests these forms may precipitate in different locations within the microbial mat. For example, the micrite may form deeper in the mat, in association with EPS, where respiration produces lower DIC $\delta^{13}\text{C}$ values. A similar conclusion was reached in a marine stromatolite study, where the authors found lower $\delta^{13}\text{C}$ values for fine-grained aragonite in the EPS compared to other grains and attributed these low values to microbial respiration (Andres et al., 2006). We also observed an association between micrite and EPS in the SEM images (Figure 3g,h), which is consistent with the conclusions made by others (Arp et al., 2012; Suarez-Gonzalez & Reitner, 2021) that the micrite is directly precipitated within the EPS of microbial mats.

Even though the origins of spherules in lacustrine and marine settings are debated, all proposed formation mechanisms suggest that spherules are formed *in situ* in the surface sediment or mat

TABLE 2 Biological processes and corresponding functional genes known to influence carbonate precipitation

Biological processes	Pathways	Carbon isotope fractionation ^a	Gene	Protein
Oxygenic photosynthesis	Photosystem	NA ^b	<i>psbA</i>	Photosystem II protein D1
			<i>psbD</i>	Photosystem II protein D2
			<i>psaA</i>	Photosystem I P700 chlorophyll a apoprotein A1
			<i>psaB</i>	Photosystem I P700 chlorophyll a apoprotein A2
Oxygenic/anoxygenic photosynthesis	Calvin cycle	-20 to -30‰	<i>rbcl</i> <i>prkB</i>	RubisCO Phosphoribulokinase
	rTCA	-2 to -12‰	<i>ACLY</i> <i>aciA</i>	ATP citrate (pro-S)-lyase ATP-citrate lyase
Anoxygenic photosynthesis	3-Hydroxypropionate bicycle (3HP)	-12.5 to -13.7‰	<i>mch</i>	2-methylfumaryl-CoA hydratase
			<i>mct</i>	2-methylfumaryl-CoA isomerase
			<i>meh</i>	3-methylfumaryl-CoA hydratase
			<i>K14469</i>	3-hydroxypropionyl-CoA synthetase
			<i>mcl</i>	methyl-CoA/(S)-citramalyl-CoA lyase
			<i>bccA</i>	acetyl-CoA/propionyl-CoA carboxylase
			<i>cooS</i>	Carbon-monoxide dehydrogenase catalytic subunit
			<i>coxS</i>	Carbon-monoxide dehydrogenase small subunit
			<i>cdhA</i>	acetyl-CoA decarboxylase/synthase complex
			<i>acsB</i>	acetyl-CoA synthase
Sulfate reduction	Dicarboxylate-4-hydroxybutyrate cycle (4HB)	-0.2 to -3.8‰	<i>abfd</i>	4-hydroxybutyryl-CoA dehydratase
			<i>cysNC</i>	Bifunctional enzyme CysN/CysC
			<i>cysD</i>	Sulfate adenylyltransferase subunit 2
			<i>dsrB</i>	Sulfite reductase beta subunit
			<i>aprA</i>	Adenylyl-sulfate reductase subunit alpha
Anaerobic methane oxidation	-	-5.2 to -31.3‰ ^d	<i>pmoA</i>	Methane monooxygenase

(Continues)

TABLE 2 (Continued)

Biological processes	Pathways	Carbon isotope fractionation ^a	Gene	Protein
Denitrification	-	NA ^c	<i>napA</i>	Periplasmic nitrate reductase
	-		<i>nirK</i>	Nitrite reductase
	-		<i>nirS</i>	Nitrite reductase
	-		<i>norB</i>	Nitric oxide reductase
	-		<i>nosZ</i>	Nitrous oxide reductase
Methanogenesis	-	-9 to -83% ^e	<i>mcrA</i>	Methyl coenzyme M reductase
Ureolysis	-	-12.5% ^f	<i>ureC</i>	Urease subunit alpha
Ammonification	-	NA ^c	<i>echA</i>	enoyl-CoA hydratase
Extracellular enzyme	-	NA ^c	<i>cynT</i>	Carbonic anhydrase

^aValues are from Berg et al. (2010), unless specifically mentioned.

^bThis process only participates in electron transfer for photosynthesis, so it would not impact the $\delta^{13}\text{C}$ fractionation.

^cThis process will generate bicarbonate from organic carbon/methane with lower $\delta^{13}\text{C}$ values, which will decrease the $\delta^{13}\text{C}$ of the DIC pool.

^dValue is from Barker and Fritz (1981).

^eDifferent types of methanogenesis (acetoclastic/hydrogenotrophic/methylotrophic) have different fractionation factors (Penger et al., 2012 and references therein).

^fValue is from Millo et al. (2012).

region given their large sizes (Arp et al., 2012; Suarez-Gonzalez & Reitner, 2021; and references therein). We find EPS-rich cavities and filaments as nucleus or laminae in our spherule samples (Figure 3c–e), suggesting *in situ* growth of their cortices related to EPS, which shows good agreement with the proposed formation mechanisms for spherules from other Kiritimati lakes (Arp et al., 2012; Schneider et al., 2013; Suarez-Gonzalez & Reitner, 2021).

Second, we consider whether these late Holocene sediments have undergone substantial diagenesis. Some common physical alteration signatures of ooids and spherules include dissolution (e.g., pitting and voids), cementation (e.g., sparite cement filling pore space, isopachous aragonitic crusts of original grains, and micritization), mineral replacement, and recrystallization (Scholle & Ulmer-Scholle, 2003). The petrographic images of spherules present evidence of borings, dissolution (pitting), micritization, isopachous crusts of fibrous aragonite cement, and recrystallization (Figure S4), suggesting that they have undergone some degree of alteration. Previous studies show that microbially mediated dissolution, such as driven by endolithic cyanobacteria, can drive small changes in $\delta^{13}\text{C}$ values of the shallow sediments, which can impact the $\delta^{13}\text{C}$ values of precipitated carbonates (Present et al., 2021). However, diagenesis is unlikely to cause significant changes in the $\delta^{13}\text{C}_{\text{carb}}$ values in our relatively young, late Holocene sediment core for the following reasons: First, evidence of diagenesis is observed consistently in both the shallowest as well as the deepest core samples (Figure S4), suggesting that alteration is likely happening syndepositionally before burial. Thus, altered carbonate likely is still recording surface, rather than porewater $\delta^{13}\text{C}$ values (Havig et al., 2018). Second, carbonate $\delta^{13}\text{C}$ values are more resistant to diagenesis than $\delta^{18}\text{O}$ values (Banner & Hanson, 1990). Our data do not show secular $\delta^{18}\text{O}$ changes beyond $\sim 0.5\%$, suggesting that alteration has been minimal (Figure 4b). Lastly, diagenesis, especially meteoric diagenesis, often leads to more negative $\delta^{13}\text{C}$ values in altered carbonates (Allan & Matthews, 1982). However, the relatively high $\delta^{13}\text{C}$ values of both spherules and micrite, and the increase in $\delta^{13}\text{C}_{\text{carb}}$ values with depth (Figures 4 and 5), are opposite to the expected impacts of increasing diagenesis with depth/time. Therefore, we seek other explanations, besides diagenesis, to explain the observed $\delta^{13}\text{C}_{\text{carb}}$ values in the sediment core.

4.2 | $\delta^{13}\text{C}$ offset between spherules and micrite: the role of the diurnal carbon cycle engine

4.2.1 | High $\delta^{13}\text{C}$ values in carbonates and metagenomic evidence of biological processes

Both $\delta^{13}\text{C}_m$ and $\delta^{13}\text{C}_{sp}$ values are significantly higher than the equilibrium aragonite $\delta^{13}\text{C}$ values calculated from the mean value of the $\delta^{13}\text{C}_{\text{DIC}}$ distributions from Kiritimati lakes (mean $\delta^{13}\text{C}_{\text{DIC}} = -1\%$, mean $\delta^{13}\text{C}_{\text{aragonite}} = 1.7\%$, Figure 5b). Therefore, it is likely that the precipitated carbonates are recording much higher local DIC $\delta^{13}\text{C}$ values, which can arise from both abiotic and biotic

processes. Abiotic processes such as CO_2 degassing from thermal springs and evaporation can cause non-equilibrium gas-transfer isotope fractionation, leading to very high $\delta^{13}\text{C}_{\text{carb}}$ values (>10‰) for precipitated carbonates in saline lake systems (Valero-Garcés et al., 1999). However, the lack of correlation of $\delta^{13}\text{C}_{\text{DIC}}$ with calculated salinity and Na concentration from the 2019 spatial survey of Kiritimati lakes suggests no clear relationship between high salinity, driven by evaporation (Wyman et al., 2021), and $\delta^{13}\text{C}_{\text{DIC}}$ (Figure S7). Thus, biological processes with significant isotope fractionation factors are more likely to lead to the observed high $\delta^{13}\text{C}$ signatures of Kiritimati carbonates. Biological processes that can induce carbonate precipitation are comprehensively discussed in the literature and include photosynthesis, carbon fixation, sulfate reduction, denitrification, anaerobic methane oxidation, methanogenesis, ammonification, and ureolysis (Berg et al., 2010; Bergmann et al., 2013; Dupraz et al., 2009; Zhu & Dittrich, 2016) (Table 2). Carbon fixation processes and methanogenesis incorporate lighter isotopes in organic carbon or CH_4 , increasing the $\delta^{13}\text{C}$ value of the remaining DIC pool and subsequently precipitated carbonates. Heterotrophic processes can have different impacts on $\delta^{13}\text{C}$ value of precipitated carbonates. On one hand, sulfate reduction and denitrification will produce bicarbonate from organic carbon, which generally has more depleted $\delta^{13}\text{C}$ values, leading to a significant decrease in the $\delta^{13}\text{C}$ values of the DIC pool and precipitated carbonates. For example, in freshwater and marine settings, respiration and sulfate reduction are hypothesized to lower $\delta^{13}\text{C}$ values of carbonate grains found in deeper layers of microbialites as well as the EPS of microbial mats (Andres et al., 2006; Nitti et al., 2012). On the other hand, anaerobic methane oxidation and ureolysis have distinctive fractionation factors that can lead to ^{13}C enrichment of DIC, thus driving higher $\delta^{13}\text{C}$ values in precipitated carbonates (Barker & Fritz, 1981; Millo et al., 2012). Given the high $\delta^{13}\text{C}$ values observed in this study, carbon fixation, methanogenesis, anaerobic methane oxidation, and ureolysis are the most likely biological processes influencing DIC $\delta^{13}\text{C}$ values.

On the surface (0–5 cm, MET-1), both taxa (Cyanobacteria) and functional genes (photosystem: *psbA/D*, *psaA/B*, Calvin cycle: *rbcL/prkB*, reductive TCA: *aclA*, and 3-hydroxypropionate bicycle: *mch*, *mcl*) related to photosynthesis (oxygenic and anoxygenic) have the highest relative abundances and are more predominant than other functional groups that can trigger carbonate precipitation (Figures 6a, b, S4). Photosynthesis increases alkalinity and pH, and some phototrophs (e.g., Cyanobacteria) can also act as nucleation sites for carbonate minerals (Dupraz et al., 2009). Additionally, photosynthesis leads to the incorporation of lighter C isotopes into organic matter, which can significantly increase the $\delta^{13}\text{C}$ values of the remaining DIC pool (Arp et al., 2012; Rosen et al., 1995), from which carbonates are precipitated. Therefore, the observed high $\delta^{13}\text{C}_{\text{carb}}$ values may result from high rates of photosynthesis that can both promote carbonate precipitation and increase $\delta^{13}\text{C}$ DIC values (e.g., Bergmann et al., 2013; Geyman & Maloof, 2019). Heterotrophic processes that can trigger carbonate production, such as sulfate reduction, ammonification,

and carbonic anhydrase activity, are also present in high abundance in the surface mat (Figure 6b). Therefore, carbonates formed in the heterotrophic layer of the microbial mat impacted by those heterotrophic processes can have distinctive $\delta^{13}\text{C}$ signatures compared to carbonates formed in the photosynthetic layers. Even though the carbon isotope fractionation caused by heterotrophic activities is either often negligible (sulfate reduction: 0–2‰) (Londry & Des Marais, 2003), or currently unknown (ammonification and carbonic anhydrase), these processes can remineralize ^{13}C -depleted OM and result in lower $\delta^{13}\text{C}_{\text{DIC}}$ values in the local environment, causing more negative $\delta^{13}\text{C}$ values for precipitated carbonates.

In the anoxic, subsurface sediments, functional genes of key enzymes (*cooS*, *coxS*, *cdhA*, *acsB*, and *abfD*) of several other carbon fixation pathways, including the Wood–Ljungdahl pathway and the dicarboxylate/4-hydroxybutyrate (4HB) cycle, are dominant (Figure 6b). The Wood–Ljungdahl pathway can use CO_2 as an electron acceptor to produce acetyl-CoA and pyruvate that can be used for biosynthesis, while the 4HB cycle can use bicarbonate (HCO_3^-) to generate acetyl-CoA and succinyl-CoA (Berg et al., 2010). Since both activities can incorporate bicarbonate and/or fix CO_2 , they can potentially influence carbonate precipitation and increase $\delta^{13}\text{C}$ DIC values (Berg et al., 2010). Therefore, these processes will increase the $\delta^{13}\text{C}$ values of precipitated carbonates derived from the porewater (Table 2). However, the Wood–Ljungdahl pathway generates acetate (CH_3COOH), which would decrease pore water alkalinity and inhibit the production of carbonate minerals. The actual impacts of such anaerobic carbon fixation on carbonate mineral formation are poorly explored, and porewater chemistry data are required to understand how these processes may influence bulk carbonate. Apart from the carbon fixation processes listed above, methanogenesis also has an extremely high $\delta^{13}\text{C}$ signature in carbonates precipitated from pore waters of anoxic environments where ^{13}C -depleted methane is generated (Gu et al., 2004). However, taxa (class Methanobacteria, Methanopyri, Methanomicrobia, and Methanococci) and the functional gene (*mcrA*) related to methanogenesis are rare in all metagenomes, which makes it unlikely to be a critical process driving the high $\delta^{13}\text{C}$ values of precipitated carbonates.

In conclusion, both taxa and functional gene results from metagenomes suggest that phototrophs, which promote carbonate precipitation and result in high $\delta^{13}\text{C}$ values in the precipitated carbonates, are abundant in the surface mat region. In addition, other functional genes related to sulfate reduction, ammonification, and carbonic anhydrase are also present and might impact the $\delta^{13}\text{C}$ values of carbonate forming in the heterotrophic layers. In deeper sediments, other anaerobic carbon fixation pathways are dominant and could impact the $\delta^{13}\text{C}$ value of the pore water, a hypothesis that requires further investigation. However, given that the primary carbonate investigated here is formed in the surface environment (in the surface mat or water column), the anaerobic carbon fixation pathways are less likely to have contributed to the elevated $\delta^{13}\text{C}$ values in our dataset.

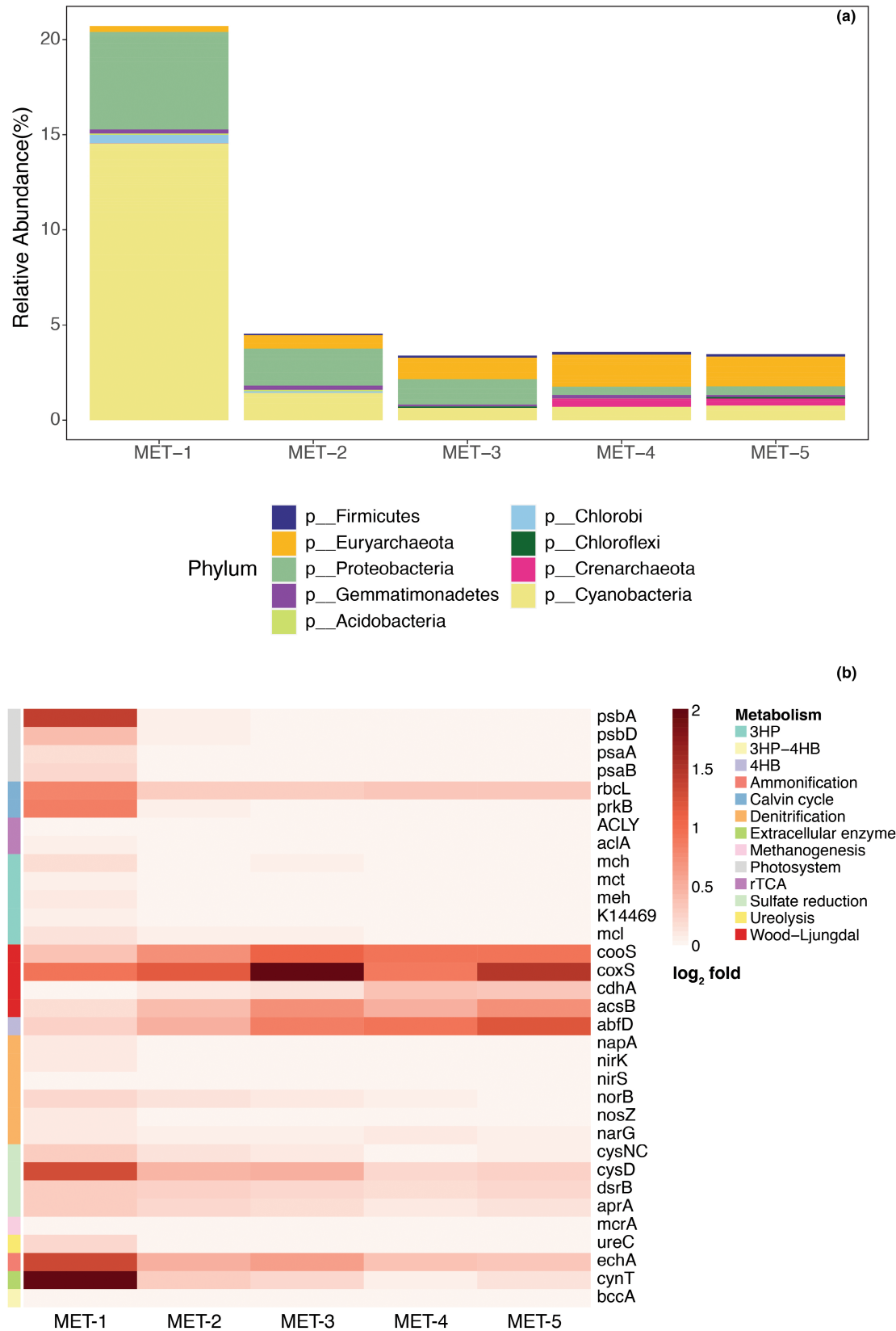


FIGURE 6 Analysis of five metagenomes of Lake 1 (MET-1: 0–5 cm, MET-2: 5–22.5 cm, MET-3: 22.5–34.2 cm, MET-4: 34.2–38 cm, and MET-5: 38–40.2 cm) showing the relative abundances of (a) microbial taxa characterized according to phylum that contain representative members associated with metabolic activities that can trigger carbonate formation and (b) microbial functional genes in candidate metabolic pathways that can yield putative effects on carbonate formation. The representative taxa were extracted from the DIAMOND-MEGAN pipeline. The results represent KO gene counts from the JGI-IMG pipeline and normalized by *rpoB* gene counts

4.2.2 | $\delta^{13}\text{C}$ offset: temporal and spatial variability of photosynthesis

Both the fine and coarse fractions of the Lake 1 sediment core have higher $\delta^{13}\text{C}$ values than predicted from $\delta^{13}\text{C}_{\text{DIC}}$ values, but the aragonitic spherules have $\delta^{13}\text{C}$ values that are $\sim 1.7\%$ higher than the micrite (median $\delta^{13}\text{C}_{\text{sp}} = 6.46\%$, median $\delta^{13}\text{C}_{\text{m}} = 4.72\%$, Figures 4b, 5b). Mineralogy differences ($\epsilon_{\text{aragonite-water}}: +2.7\%$, $\epsilon_{\text{calcite-water}}: +1\%$, Romanek et al., 1992) cannot explain the observed offset. The mineral composition of the micrite is predominantly aragonite (86.2%), whereas the spherules are 100% aragonite. The differences in mineral composition should thus lead to a 0.23‰ difference in $\delta^{13}\text{C}$ values, an offset much lower than observed (average $\delta^{13}\text{C}_{\text{sp}} - \delta^{13}\text{C}_{\text{m}} = 1.74\%$). Moreover, any external forcing on lake water DIC would likely change the $\delta^{13}\text{C}_{\text{m}}$ and $\delta^{13}\text{C}_{\text{sp}}$ values in the same direction, rather than varying the magnitude of the offset between the two grain-size fractions. We propose that biological processes and differences in the timing and location of carbonate precipitation impact the $\delta^{13}\text{C}$ values of one carbonate grain fraction relative to the other. Given that the phototrophs and heterotrophs that can trigger carbonate precipitation are both dominant in the surface mat, we propose that spherules form during peak photosynthetic forcing in the photosynthetic region of the mat. In contrast, the micrite forms more consistently in the heterotrophic layer of the mat and/or in the water column, leading to significantly higher $\delta^{13}\text{C}$ values of spherules relative to the micrite and producing the observed offset in $\delta^{13}\text{C}$ values.

Our modeling results and the related conceptual model of the diurnal carbon engine (Geyman & Maloof, 2019) provide support for a temporal interpretation of the carbonate $\delta^{13}\text{C}$ values and offset in our lake system (Figure 8). Spherules grow embedded within the microbial mats of Kiritimati lakes (Arp et al., 2012; Schneider et al., 2013). Even though EPS inhibits the nucleation of carbonate minerals, this inhibition can be overcome during peak photosynthesis (Arp et al., 2012). Given the abundant oxygenic phototrophs (Cyanobacteria, 14.5%) and consistently high spherule $\delta^{13}\text{C}$ values (5.31‰–8.11‰), we propose that spherules form primarily during the hours around peak photosynthesis ($\sim 15:00$) in the top mat layer of Lake 1. During this time, the mat DIC pool $\delta^{13}\text{C}$ values would be at their diurnal maximum, resulting in high $\delta^{13}\text{C}$ values of precipitated carbonates. Micrite precipitation could occur either (1) in the water column, as lake water is supersaturated with respect to aragonite and calcite, or (2) in the lower layer of the microbial mat, where degradation of EPS can promote carbonate production (Dupraz et al., 2009). Given the consistent positive carbonate fluxes across the day (Figure S2), micrite may be able to precipitate more consistently in the water column throughout a diurnal cycle without restrictions from EPS, and thus record a signal closer to the time-averaged $\delta^{13}\text{C}$ values of the water column/microbial mat DIC pool. Additionally, for micrite forming in the lower layers of the microbial mat, the remineralization of ^{13}C -depleted OM can lower $\delta^{13}\text{C}$ values of the local DIC pool and result in lower $\delta^{13}\text{C}$ values (Andres et al., 2006). Both microbial communities and functional genes related to heterotrophy are present in the metagenome of the

surface mat (Figure 6). In addition, FAPROTAX results also show high relative abundances of both phototrophy and aerobic chemoheterotrophy in the surface mat (Figure S8).

Our geochemical modeling also indicates that the high observed $\delta^{13}\text{C}_{\text{sp}}$ values are an indicator of high photosynthetic forcing ($\kappa_p = 600 \mu\text{mol/kg}$) with restricted precipitation hours around peak photosynthesis (2 h, 14:00–16:00) (Figure 7a). Changing precipitation hours around peak photosynthesis to 24 hours leads to a 1.2‰ decrease in simulated $\delta^{13}\text{C}_{\text{carb}}$ values using the same κ_p (Figure 7a). In conclusion, the high $\delta^{13}\text{C}$ values of spherules are likely a result of high photosynthetic forcing and constrained precipitation timing during peak photosynthesis. In contrast, the relatively lower $\delta^{13}\text{C}$ values of the micrite can result from both consistent production throughout the day and night and/or precipitation in the heterotrophic layers of the microbial mat, where local DIC $\delta^{13}\text{C}$ values would be relatively depleted. Future studies, including a finer-scale sampling of the microbial mat and attached carbonate grains, will be able to provide better constraints on the formation of carbonate in this system.

In addition to the diurnal controls of carbonate precipitation, seasonal-to-interannual changes in the physiochemical conditions of lake water may also influence the $\delta^{13}\text{C}$ values of lake water DIC and the precipitated carbonate fractions. We have observed substantial interannual variability in the physiochemical conditions of Lake 1 (Table 1), and many of the changes are linked to changes in precipitation and groundwater flow driven by El Niño–Southern Oscillation events (Higley & Conroy, 2019; Wyman et al., 2021). Groundwater often has low $\delta^{13}\text{C}$ values ($< -10\%$) compared to our lake water due to the microbial respiration of organic carbon and the subsequent reactions with marine carbonate rock (Deines et al., 1974). On Kiritimati, $\delta^{13}\text{C}_{\text{DIC}}$ values from nearby, groundwater-fed Lake 30 were as low as -11.81% in 2019, when salinity was close to 0 (1.7 ppt) and high groundwater flow into the lake was observed, with the lake as an effectively open system with short residence time (Wyman et al., 2021). The addition of groundwater with such low $\delta^{13}\text{C}$ values to Lake 1 could lower the $\delta^{13}\text{C}$ values of the DIC pool and cause more negative $\delta^{13}\text{C}$ values for all precipitated carbonates. Our model did not include groundwater due to the lack of constraints on the groundwater flow rate for Lake 1 and the lack of groundwater DIC/TA measurements. When using nearby Lake 30 groundwater values (TA = 6510.6 $\mu\text{mol/kg}$, DIC = 6390.2 $\mu\text{mol/kg}$, $\delta^{13}\text{C}_{\text{DIC}} = -11.81\%$) and considering a dry year condition (2017) with low groundwater flow rate (0.00023 $\text{kg/m}^2/\text{s}$), the simulated $\delta^{13}\text{C}_{\text{carb}}$ values (-0.07 – 0.61%) are lower compared to a simulation with no groundwater (3.23–3.77‰, Table S7). These simulated $\delta^{13}\text{C}$ values also are lower than any measured spherule carbonate (5.31–8.11‰), not to mention that wet-year conditions with higher groundwater fluxes would lead to even more negative $\delta^{13}\text{C}_{\text{carb}}$ values. Also, while the groundwater flux affects the mean $\delta^{13}\text{C}_{\text{carb}}$ values, it has little impact on the $\delta^{13}\text{C}$ offset between micrite and spherules (0.04–0.68‰ for the groundwater condition vs. 0.02–0.53‰ for the no groundwater condition, Table S7). Additionally, groundwater often has a much lower pH than lake water, resulting in undersaturated conditions for carbonate minerals (Table S5). Thus, an increase in groundwater flux could hinder mineral precipitation in this lake (Singurindy et al., 2004).

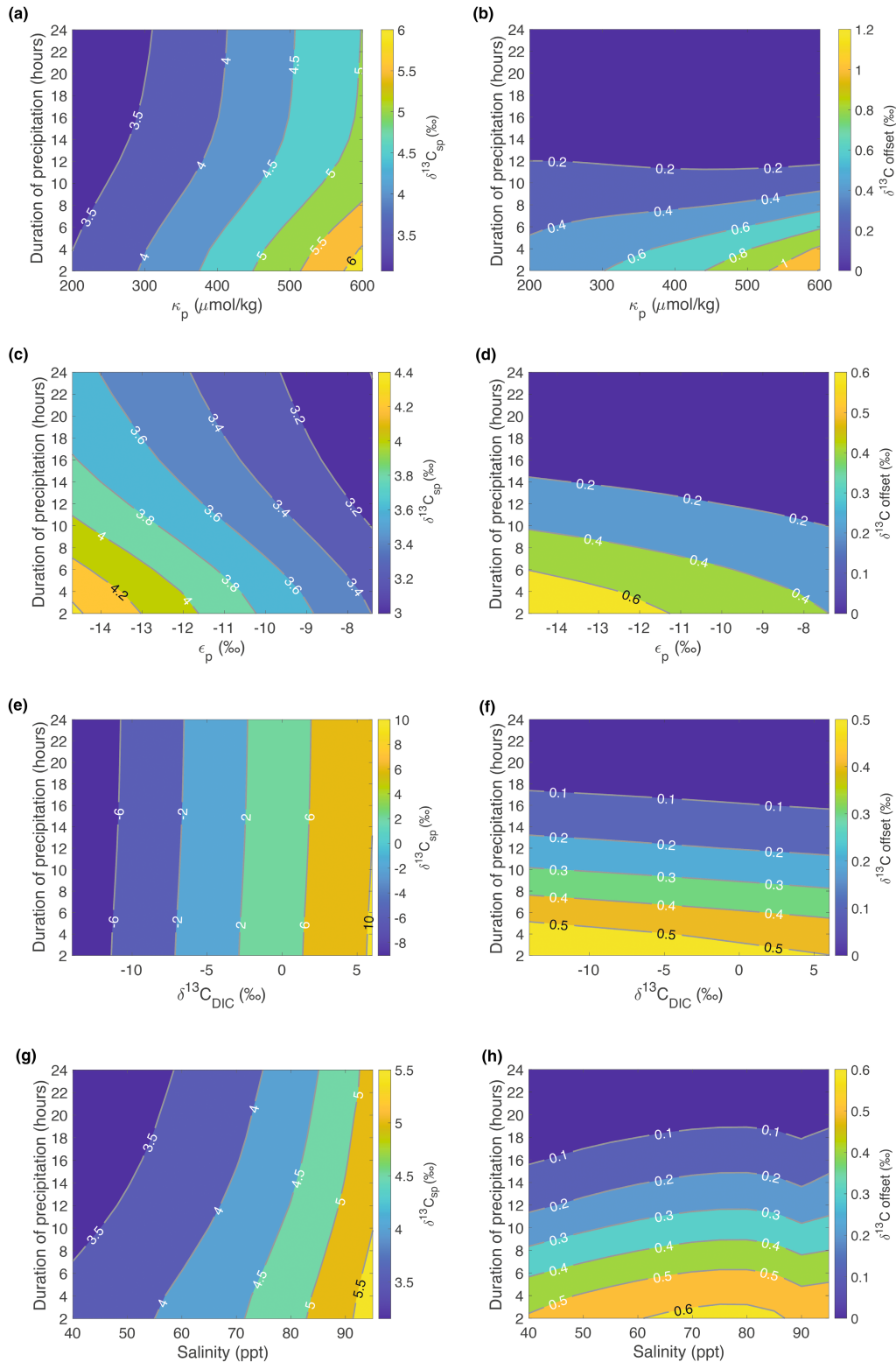


FIGURE 7 Contour maps for simulated $\delta^{13}\text{C}_{\text{sp}}$ (first column) and the $\delta^{13}\text{C}$ offset between precipitated carbonates and mean (time-averaged) DIC (second column) under a variety of forcing conditions. The y-axis records the number of hours of the day when carbonate precipitation is occurring (duration of precipitation hours). In our simulations, the carbonate saturation state is >1 during all hours of the day. However, as a sensitivity test, we explore what happens when precipitation only occurs for 2–24 h around “peak photosynthesis,” which occurs at 15:00, according to a compilation of water chemistry measurements from 21 shallow marine carbonate environments (Geyman & Maloof, 2019). We simulate the $\delta^{13}\text{C}_{\text{sp}}$ and $\delta^{13}\text{C}$ offset when changing (a,b) κ_p , (c,d) ϵ_p , (e,f) the initial $\delta^{13}\text{C}_{\text{DIC}}$, and (g,h) salinity. $\delta^{13}\text{C}_{\text{sp}}$ represents the simulated $\delta^{13}\text{C}_{\text{carb}}$ values using mineral composition of spherules, κ_p is the diurnal organic carbon transfer, and ϵ_p is the isotopic fractionation for photosynthesis. Other input parameters are kept the same for each sensitivity test

We thus conclude that seasonal and interannual variability in ground-water flux is unlikely to be the main cause of both the high $\delta^{13}\text{C}_{\text{carb}}$ values and the observed $\delta^{13}\text{C}$ offset in this lake system.

In other hypersaline systems, microbial mats show periodic growth and decay phases linked to salinity, which sometimes result in different carbonate mineralogy (Cabestrero et al., 2018). Therefore, it also is possible that spherules precipitate only during periods of active microbial mat growth, when the high alkalinity helps to overcome the inhibitory effects of EPS. In this scenario, the spherules would preferentially record the higher values of water column $\delta^{13}\text{C}_{\text{DIC}}$ caused by intense photosynthesis. In contrast, during periods of microbial mat decay (dominated by anoxygenic phototrophs and heterotrophs), the micrite could continue to precipitate even while spherule growth is inhibited by the EPS. In this case, the dominant heterotrophic activity would decrease water column $\delta^{13}\text{C}_{\text{DIC}}$ causing the micrite to have lower average $\delta^{13}\text{C}$ values (Gu et al., 2006). Recent studies of Kiritimati ooids suggest the radial fibrous lamina of ooids is formed during intense photosynthesis with rapid precipitation, whereas the micritic laminae are formed by EPS-controlled mechanisms in intervening periods without intense photosynthesis (Suarez-Gonzalez & Reitner, 2021). As our microbial mat has relatively young radiocarbon dates (130 cal yr BP at the bottom), as well as being photosynthetically active without multiple layers, it provides a perfect analogy to other photosynthetically active microbial mats in Lake 21 where only non-laminated ooids are found (Suarez-Gonzalez & Reitner, 2021). Additionally, many of our spherules (in both surface and deeper sections) in Lake 1 do not contain multiple micritic laminae (Figure 3), further supporting that those spherules are likely growing rapidly only in the phototrophic layer of the microbial mat during intense photosynthesis, thus recording high $\delta^{13}\text{C}$ values of the lake's DIC. When multiple laminae are present in spherules, it is possible that they have multiple growth cycles representing seasonal or even interannual periods, which influence the water chemistry and biology of the lake. For example, interannual El Niño events cause high precipitation rates on Kiritimati Island and decrease the salinity of its lakes. As a result, the photosynthesis could become even more intense and favor the formation of radial laminae even more. During La Niña years and neutral states, the higher salinity of the lakes likely leads to weaker photosynthesis, which can promote the formation of micritic laminae of the spherules. In summary, the same temporal interplay between photosynthesis and respiration described by the diurnal carbon engine (section 2.6; Geyman & Maloof, 2019) may occur on longer (e.g., seasonal or interannual) timescales.

4.3 | Interpreting time series of geochemical variables in Lake 1: $\delta^{13}\text{C}$ offset as a potential paleoproductivity indicator

Geochemical variables measured in the Lake 1 sediment core show pronounced variability over the last 1500 years (Figure 4b). $\delta^{13}\text{C}_{\text{sp}}$ values remain high from 1500 cal yr BP to present (averaging 6.56‰),

with even higher values before 1170 cal yr BP (averaging 7.45‰), whereas $\delta^{13}\text{C}_{\text{m}}$ values are lower from 452 cal yr BP to present (averaging 1.98‰) compared to 1411 to 452 cal yr BP (averaging 4.86‰, two-tailed *t*-test, $p < .001$). The $\delta^{18}\text{O}_{\text{sp}}$ time series demonstrates an increasing trend of ~1‰ over the last 1,500 years (Figure 4b). The $\delta^{18}\text{O}_{\text{m}}$ time series, on the other hand, does not show a clear increasing or decreasing trend. $\delta^{13}\text{C}_{\text{org}}$ shows a decreasing trend from 1411 to 974 cal yr BP (from -10.53‰ to -18.26‰), and increases from around 974 cal yr BP to present (from -18.26‰ to -14.25‰). The $\delta^{13}\text{C}$ offset, total organic carbon (TOC), and total nitrogen (TN) have similar patterns, with significantly higher values from 452 cal yr BP to present and 1411 to 1297 cal yr BP (averaging 3.51‰, 2.94%, and 0.31%, respectively) compared to 1297 to 452 cal yr BP (averaging 2.03‰, 1.44%, and 0.16%, respectively, two-tailed *t*-test, $p < .005$ for $\delta^{13}\text{C}$ offset, $p < .001$ for TOC and TN). We evaluate the potential implications of variability in $\delta^{18}\text{O}$, $\delta^{13}\text{C}$, the correlation of $\delta^{13}\text{C}$ - $\delta^{18}\text{O}$, and the $\delta^{13}\text{C}$ offset in the context of past environmental changes below.

Both the spherules and micrite have significant correlations between $\delta^{18}\text{O}_{\text{carb}}$ and $\delta^{13}\text{C}_{\text{carb}}$ ($r = 0.60$ and 0.75 , $N = 17$, $p < .05$ and $p < .001$, respectively). Generally, significant correlations between carbonate $\delta^{18}\text{O}$ and $\delta^{13}\text{C}$ values are found in hydrologically closed basin lakes (Talbot, 1990). The majority of lakes in Kiritimati are considered closed systems due to the substantial differences in lake levels even between adjacent lakes (Helfrich et al., 1973), although there is clearly subsurface hydrological flow in some lakes (Wyman et al., 2021). For both spherules and matrix, the variations in $\delta^{18}\text{O}$ values are smaller compared to $\delta^{13}\text{C}$ values, resulting in a steeper slope (>1) of $\delta^{13}\text{C}_{\text{carb}}/\delta^{18}\text{O}_{\text{carb}}$ (Figure 5a). This could suggest that local biological mediation of carbonate chemistry (greater change in $\delta^{13}\text{C}$) has a greater impact on the carbonate formation than hydroclimate change (greater change in $\delta^{18}\text{O}_{\text{carb}}$) (Ingalls et al., 2020), highlighting biological processes as critical to the formation of carbonate in this system.

In the sediment core, we also observed significantly higher $\delta^{18}\text{O}$ values of spherules relative to micrite ($p < .00001$, paired *t*-test result). Lacustrine carbonate $\delta^{18}\text{O}$ values are often interpreted as proxies of precipitation minus evaporation (P-E) since they represent changes in lake water $\delta^{18}\text{O}$ values, controlled by lake hydrology and moisture balance (Leng & Marshall, 2004). However, studies of Lake 30 carbonate $\delta^{18}\text{O}$ values in Kiritimati show no correlation with reconstructed salinity over the last millennium (Wyman et al., 2021). Additionally, the Kiritimati lake water $\delta^{18}\text{O}$ values measured in the 2019 spatial survey are not correlated with salinity ($r = 0.18$, $p = .34$, $N = 31$). With extremely high salinity, the thermodynamic activity of water decreases, resulting in lower kinetic fractionation and reducing the subsequent increase in the $\delta^{18}\text{O}$ values of the residual water (Gonfiantini, 1986). Therefore, periodically hypersaline conditions of Lake 1 may obscure the P-E signal in lake water and carbonate $\delta^{18}\text{O}$ values. However, the $\delta^{18}\text{O}$ offset between syndepositional spherules and micrite supports potential temporal and spatial disparities in their precipitation. Unlike $\delta^{13}\text{C}_{\text{DIC}}$ that often shows an apparent diurnal cycle (e.g., Richardson et al., 2017), lake $\delta^{18}\text{O}_{\text{w}}$ values are not expected to vary diurnally in such a pronounced manner, given lake water residence times are on the order of days to months

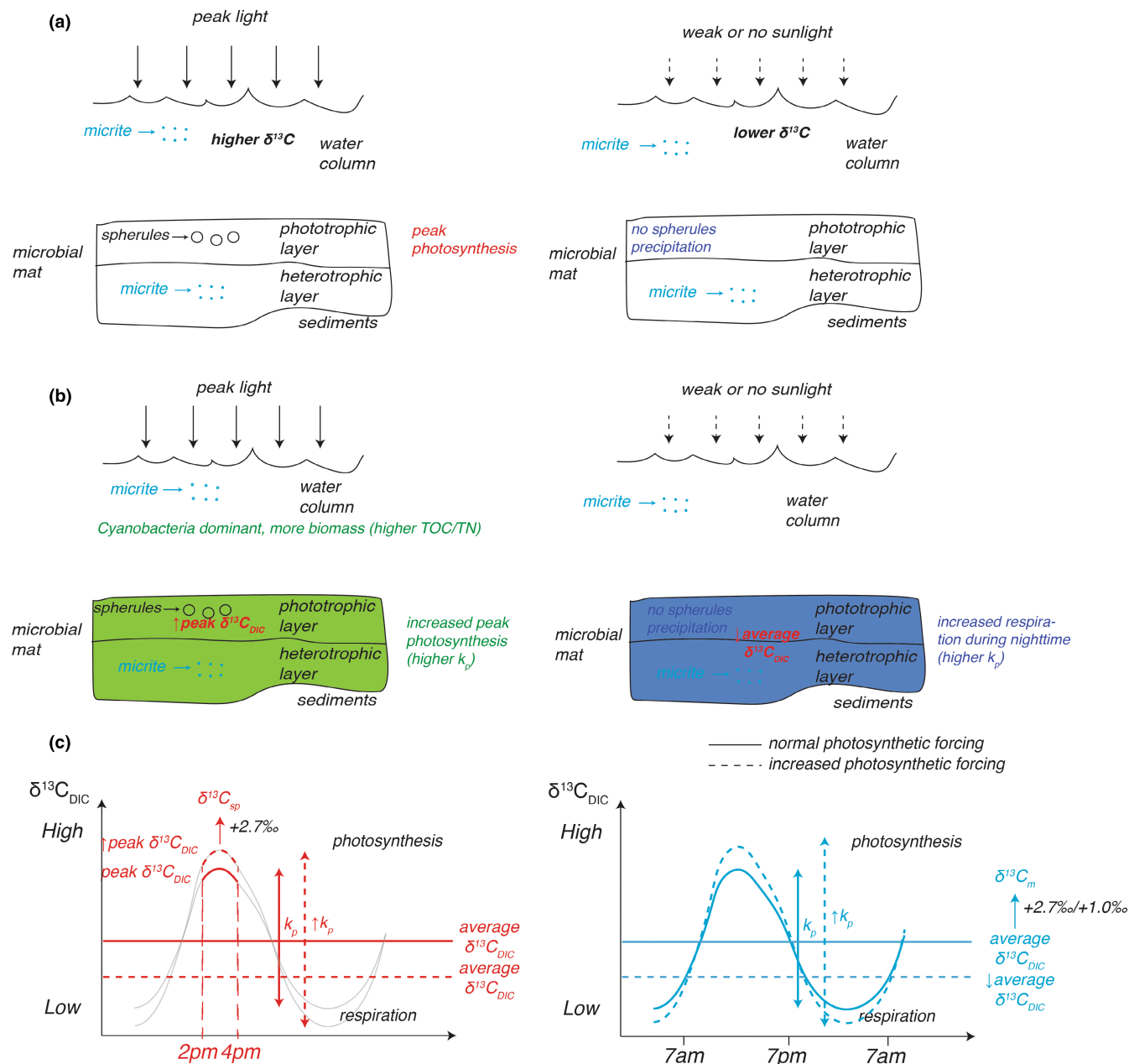


FIGURE 8 (a) Conceptual models of spherule and matrix precipitation in Lake 1. During peak photosynthesis, the $\delta^{13}\text{C}_{\text{DIC}}$ within the uppermost mat will increase and the saturation state of aragonite will also increase, resulting in precipitated spherules with higher $\delta^{13}\text{C}$ values. Micrite, which precipitates more consistently in the water column and in deeper layers of the surface mat will record a $\delta^{13}\text{C}$ value that is closer to the average $\delta^{13}\text{C}_{\text{DIC}}$ of the system through time, or lower due to increased respiration deeper in the mat. (b) Conceptual models for spherule and micrite precipitation in Lake 1 under higher photosynthetic forcing. In this scenario, the peak $\delta^{13}\text{C}_{\text{DIC}}$ will be higher, resulting in higher $\delta^{13}\text{C}_{\text{sp}}$. However, higher intensity of respiration at night may result in relatively lower $\delta^{13}\text{C}$ values of the precipitated micrite. (c) Conceptual models showing diurnal and average $\delta^{13}\text{C}_{\text{DIC}}$ changes under different photosynthetic forcing conditions, which are recorded by the $\delta^{13}\text{C}$ values of precipitated spherules and micrite

to years, rather than hours. However, seasonal-to-interannual fluctuations of lake water $\delta^{18}\text{O}_{\text{w}}$ values could be recorded if spherules and micrite preferentially precipitate at different times. Measured Lake 1 temperatures (29.7–31.9°C) and $\delta^{18}\text{O}_{\text{w}}$ (1.47–2.66‰) from different field seasons would lead to $\sim 1.2\text{‰}$ changes in carbonate $\delta^{18}\text{O}$ values which are comparable to the observed $\delta^{18}\text{O}$ differences (median value $+0.44\text{‰}$). But again, these changes would impact both spherules and micrite in a similar manner, unless the micrite formed in

warmer periods or with lower $\delta^{18}\text{O}_{\text{w}}$, and spherules formed in cooler periods or with higher $\delta^{18}\text{O}_{\text{w}}$. Lake water is generally warmer during peak photosynthesis, which would lead to lower $\delta^{18}\text{O}$ values for precipitated spherules. However, the $\delta^{18}\text{O}$ values of spherules are significantly higher compared to micrite. One possible explanation for this observation is that the evaporation during peak photosynthesis swamps temperature, increasing $\delta^{18}\text{O}_{\text{w}}$ and $\delta^{18}\text{O}_{\text{carb}}$ values. Another possible explanation is that the diurnal temperature changes in the

microbial mat are more muted compared to the changes in the lake water. Therefore, the $\delta^{18}\text{O}$ offset between spherules and micrite supports the hypothesis that these two carbonate constituents form in different time periods with different $\delta^{18}\text{O}_w$ and lake temperatures, along with different rates of photosynthetic forcing.

Carbonate $\delta^{13}\text{C}$ values have been used to predict biological productivity in lacustrine settings (Talbot, 1990) and oceanic productivity and circulation in marine environments (Maslin & Swann, 2006). Thus, we expect to see a positive correlation between carbonate $\delta^{13}\text{C}$ values and other proxies used to indicate past productivity in lake sediments like TOC and TN (Talbot et al., 2006). However, the highest carbonate $\delta^{13}\text{C}$ values for both spherules and micrite do not coincide with the highest TOC and TN values, more direct archives of productivity that remain preserved in this relatively young sedimentary record (Figure 4b). Furthermore, $\delta^{13}\text{C}_{\text{sp}}$ values show no significant correlation with TOC ($r = -0.47, p > .05, N = 17$), and a slight negative correlation with TN ($r = -0.51, p = .03, N = 17$). $\delta^{13}\text{C}_m$ values also show a negative correlation with both TOC ($r = -0.68, p < .01, N = 17$) and TN ($r = -0.70, p < .01, N = 17$). On the contrary, the $\delta^{13}\text{C}$ offset between spherules and micrite shows a different pattern across the sediment record, with higher values in 1411 to 1297 cal yr BP and 452 cal yr BP to present, and lower values in 1297 to 452 cal yr BP (Figure 4b). TOC also shows similar temporal patterns of change in the sediment core and positively covaries with the $\delta^{13}\text{C}$ offset ($r = 0.57, p = .02, N = 17$), as does TN ($r = 0.57, p = .02, N = 17$). Given the observed covariations of the $\delta^{13}\text{C}$ offset with productivity proxies, we hypothesize that the $\delta^{13}\text{C}$ offset records temporal primary productivity changes in this lacustrine system.

During periods with higher gross primary productivity, increased photosynthetic forcing would increase the amplitude of the diurnal $\delta^{13}\text{C}_{\text{DIC}}$ cycle, so the peak value of $\delta^{13}\text{C}_{\text{DIC}}$ recorded by the spherules would be higher. However, the increase in respiration that accompanies increased gross primary productivity would also decrease the $\delta^{13}\text{C}_{\text{DIC}}$ values at night and below the surface layer of the mat (Nitti et al., 2012), leading to lower micrite $\delta^{13}\text{C}$ values if it forms throughout the day and night or in the deeper layers of the mat, ultimately increasing the $\delta^{13}\text{C}$ offset. This model may also extend to seasonal and interannual timescales, if, for example, photosynthetic forcing is higher during a given season or ENSO event. The sensitivity tests for the $\delta^{13}\text{C}$ offset supports this hypothesis, as the $\delta^{13}\text{C}$ offset is only sensitive to changes in the photosynthetic forcing (Figure 7b), while other parameters that can significantly change the $\delta^{13}\text{C}_{\text{sp}}$ (e.g., the initial $\delta^{13}\text{C}_{\text{DIC}}$) have little influence on the $\delta^{13}\text{C}$ offset (Figure 7f). Therefore, the $\delta^{13}\text{C}$ offset can be impacted by the amplitude of the photosynthetic forcing, which can have diurnal-to-seasonal-to-interannual fluctuations, and the timing of carbonate precipitation.

Note the TOC and TN patterns observed in the Lake 1 sediment core (Figure 4) could be influenced by microbial metabolic activities such as autotrophic phototrophy and heterotrophic respiration taking place at different depths in the core (e.g., Oni et al., 2015). However, we think it is unlikely that such microbial activities are the main drivers of the TOC and TN patterns in Figure 4 for the following reasons. First, we did not see significant covariations of TOC

and TN with the relative abundances of autotrophic and heterotrophic activities obtained from FAPROTAX results (Table S8). Second, FAPROTAX results indicate that chemoheterotrophy (24.5%) is dominant among the metabolisms in the deep sediment (40.2 cm; Figure S8), so we would expect to see relatively low TOC and TN in this section if TOC and TN were significantly impacted by active microbial processes in the sediment core. To the contrary, we observed some of the highest TOC (3.87%) and TN (0.39%) concentrations in the deep sediment (Figure 4). In summary, the FAPROTAX results support the conclusion that the observed TOC and TN trends in Figure 4 do not simply record current microbial processes at different sediment depths, but rather archive the change over time in paleoenvironmental conditions (e.g., paleoproductivity), in line with their typical interpretation in paleolimnologic studies.

From a geological perspective, high $\delta^{13}\text{C}$ values in marine carbonates often are linked to enhanced net productivity and carbon burial (Kump & Arthur, 1999). However, multiple processes, including local platform processes as well as marine and meteoric diagenesis, can decouple carbonate $\delta^{13}\text{C}$ values from that of the global ocean (e.g., Geyman & Maloof, 2021). Here, we have demonstrated that analyzing $\delta^{13}\text{C}$ variability of different carbonate constituents produced in the same stratigraphic intervals may help to constrain the role of local $\delta^{13}\text{C}$ processes. In this work, the $\delta^{13}\text{C}$ values of aragonite spherules and micrite are not correlated with productivity proxies such as TOC and TN, but one may potentially use the $\delta^{13}\text{C}$ offset as a better indicator of gross paleoproductivity. Thus, the $\delta^{13}\text{C}$ offset allows us to deconvolve the intensity of local biological processes in this particular environment, whereas the individual $\delta^{13}\text{C}$ values alone do not provide such information. Potential applications of the $\delta^{13}\text{C}$ offset could include investigating paleoproductivity in the carbonate rock record, where spherules or other coarse-grained forms and micrite co-occur in the same units (e.g., Cretaceous pre-salt lacustrine deposits, Pleistocene coralline reef units, and hydrothermal travertine systems Guo & Riding, 1992; Chafetz et al., 2018; Jaramillo-Vogel et al., 2019; Della Porta et al., 2022).

5 | CONCLUSION

In the sedimentary record of a near-marine hypersaline lake on Kiritimati, abundant aragonite spherules and micrite co-occur in the same sedimentary layers. However, these syndepositional carbonates have significantly different $\delta^{13}\text{C}$ values that cannot be explained by differences in mineral composition alone. To explain the anomalously high $\delta^{13}\text{C}$ values in the spherules, we hypothesize that the spherule fraction forms preferentially during peak photosynthesis, whereas the micrite fraction forms in the mat or the water column more consistently throughout diurnal and/or annual timescales. Metagenome results suggest that photosynthesis plays a dominant role in facilitating carbonate production in the surface mat. Even though some anaerobic carbon-fixation pathways are relatively abundant in the deep sediments, their participation in carbonate production remains elusive and is likely limited due to the lower pH and undersaturated

carbonate mineral conditions of porewater (Arp et al., 2012; Schneider et al., 2013). Geochemical modeling suggests that different durations of diurnal precipitation, coupled with changes in photosynthetic intensity, can lead to substantial changes in the $\delta^{13}\text{C}$ values of precipitated carbonates. Our findings further support the idea that localized intense photosynthesis can lead to high $\delta^{13}\text{C}$ values in the carbonate rock record (Geyman & Maloof, 2019). The $\delta^{13}\text{C}$ offset between syndepositional spherule and micrite $\delta^{13}\text{C}$ values, which is sensitive mainly to changes in photosynthetic forcing and covaries with primary productivity proxies such as TOC and TN, may serve as a better proxy of past primary productivity than the $\delta^{13}\text{C}$ values of individual carbonate fractions, or bulk carbonate $\delta^{13}\text{C}$ values.

ACKNOWLEDGMENTS

This research was funded by ACS-PRF 57417-DNI2 and NSF-EAR 1602590 to JLC. We thank the Environmental Ministry of the Republic of Kiribati for the research permit to complete this work. We thank A. Wyman, M. Higley, C. Karamperidou, N. Murray, and N. Meghani for field assistance, C Field, M. Band, and G. Rendon for the technical support, and A. Maloof, B. Fouke, and T. Johnson for valuable comments and advice. We thank the UIUC Roy J. Carver Biotechnology Center, specifically the High-throughput Sequencing and Genotyping Unit, for DNA sample analysis. Sequence data were produced by the US Department of Energy Joint Genome Institute (<http://www.jgi.doe.gov/>) in collaboration with the user community. We thank the editor and two anonymous reviewers for helping to improve this manuscript.

CONFLICT OF INTEREST

The authors have no conflict of interest to report.

DATA AVAILABILITY STATEMENT

The data that support the findings of this study are available from the corresponding author upon reasonable request.

ORCID

Mingfei Chen  <https://orcid.org/0000-0002-6281-2480>

Jessica L. Conroy  <https://orcid.org/0000-0003-3652-3199>

Emily C. Geyman  <https://orcid.org/0000-0003-4349-9350>

REFERENCES

- Allan, J. R., & Matthews, R. K. (1982). Isotope signatures associated with early meteoric diagenesis. *Sedimentology*, 29, 797–817. <https://doi.org/10.1111/J.1365-3091.1982.TB00085.X>
- Andres, M. S., Sumner, D. Y., Reid, R. P., & Swart, P. K. (2006). Isotopic fingerprints of microbial respiration in aragonite from Bahamian stromatolites. *Geology*, 34, 973–976. <https://doi.org/10.1130/G22859A.1>
- Arp, G., Helms, G., Karlinska, K., Schumann, G., Reimer, A., Reitner, J., & Trichet, J. (2012). Photosynthesis versus exopolymer degradation in the formation of microbialites on the atoll of Kiritimati, Republic of Kiribati, Central Pacific. *Geomicrobiology Journal*, 29, 29–65. <https://doi.org/10.1080/01490451.2010.521436>
- Bade, D. L., Carpenter, S. R., Cole, J. J., Hanson, P. C., & Hesslein, R. H. (2004). Controls of $\delta^{13}\text{C}$ -DIC in lakes: Geochemistry, lake metabolism, and morphometry. *Limnology and Oceanography*, 49, 1160–1172. <https://doi.org/10.4319/LO.2004.49.4.1160>
- Banner, J. L., & Hanson, G. N. (1990). Calculation of simultaneous isotopic and trace element variations during water-rock interaction with applications to carbonate diagenesis. *Geochimica et Cosmochimica Acta*, 54, 3123–3137. [https://doi.org/10.1016/0016-7037\(90\)90128-8](https://doi.org/10.1016/0016-7037(90)90128-8)
- Barker, J. F., & Fritz, P. (1981). Carbon isotope fractionation during microbial methane oxidation. *Nature*, 293, 289–291. <https://doi.org/10.1038/293289a0>
- Berg, I. A., Kockelkorn, D., Ramos-Vera, W. H., Say, R. F., Zarzycki, J., Hügler, M., Alber, B. E., & Fuchs, G. (2010). Autotrophic carbon fixation in archaea. *Nature Reviews Microbiology*, 8, 447–460. <https://doi.org/10.1038/nrmicro2365>
- Bergmann, K. D., Grotzinger, J. P., & Fischer, W. W. (2013). Biological influences on seafloor carbonate precipitation. *PALAIOS*, 28, 99–115. <https://doi.org/10.2110/PALO.2012.P12-088R>
- Bethke, C. M., Farrell, B., & Sharifi, M. (2020). *The Geochemist's Workbench, version 14.0: GWB essentials guide* (p. 196). Aqueous Solutions LLC.
- Blaauw, M., & Christen, J. A. (2011). Flexible paleoclimate age-depth models using an autoregressive gamma process. *Bayesian Analysis*, 6, 457–474. <https://doi.org/10.1214/11-BA618>
- Buchfink, B., Xie, C., & Huson, D. H. (2014). Fast and sensitive protein alignment using DIAMOND. *Nature Methods*, 12, 59–60. <https://doi.org/10.1038/nmeth.3176>
- Cabestrero, Ó., Sanz-Montero, M. E., Arregui, L., Serrano, S., & Visscher, P. T. (2018). Seasonal variability of mineral formation in microbial mats subjected to drying and wetting cycles in alkaline and hypersaline sedimentary environments. *Aquatic Geochemistry*, 24, 79–105. <https://doi.org/10.1007/S10498-018-9333-2>
- Chafetz, H., Barth, J., Cook, M., Guo, X., & Zhou, J. (2018). Origins of carbonate spherulites: Implications for Brazilian Aptian pre-salt reservoir. *Sedimentary Geology*, 365, 21–33. <https://doi.org/10.1016/j.sedgeo.2017.12.024>
- Chen, I.-M. A., Chu, K., Palaniappan, K., Pillay, M., Ratner, A., Huang, J., Huntemann, M., Varghese, N., White, J. R., Seshadri, R., Smirnova, T., Kirton, E., Jungbluth, S. P., Woyke, T., Eloë-Fadrosch, E. A., Ivanova, N. N., & Kyrpides, N. C. (2019). IMG/M v.5.0: an integrated data management and comparative analysis system for microbial genomes and microbiomes. *Nucleic Acids Research*, 47, D666–D677. <https://doi.org/10.1093/nar/gky901>
- Chen, M., Conroy, J. L., Sanford, R. A., Chee-Sanford, J. C., & Connor, L. M. (2020). Interpreting lacustrine bulk sediment $\delta^{15}\text{N}$ values using metagenomics in a tropical hypersaline lake system. *Journal of Paleolimnology*, 65, 151–168. <https://doi.org/10.1007/S10933-020-00157-7>
- Cohen, A., Palacios-Fest, M., Negrini, R., Wigand, P., & Erbes, D. (2000). A paleoclimate record for the past 250,000 years from Summer Lake, Oregon, USA: II. Sedimentology, paleontology and geochemistry. *Journal of Paleolimnology*, 24, 151–182. <https://doi.org/10.1023/A:1008165326401>
- Deines, P., Langmuir, D., & Harmon, R. S. (1974). Stable carbon isotope ratios and the existence of a gas phase in the evolution of carbonate ground waters. *Geochimica et Cosmochimica Acta*, 38, 1147–1164. [https://doi.org/10.1016/0016-7037\(74\)90010-6](https://doi.org/10.1016/0016-7037(74)90010-6)
- Della Porta, G., Hoppert, M., Hallmann, C., Schneider, D., & Reitner, J. (2022). The influence of microbial mats on travertine precipitation in active hydrothermal systems (Central Italy). *The Depositional Record*, 8, 165–209. <https://doi.org/10.1002/DEP2.147>
- Dupraz, C., Reid, R. P., Braissant, O., Decho, A. W., Norman, R. S., & Visscher, P. T. (2009). Processes of carbonate precipitation in modern microbial mats. *Earth-Science Reviews*, 96, 141–162. <https://doi.org/10.1016/j.earscirev.2008.10.005>
- Gaujoux, R., & Seoighe, C. (2010). A flexible R package for nonnegative matrix factorization. *BMC Bioinformatics*, 11, 1–9. <https://doi.org/10.1186/1471-2105-11-367>

- Geyman, E. C., & Maloof, A. C. (2019). A diurnal carbon engine explains ^{13}C -enriched carbonates without increasing the global production of oxygen. *Proceedings of the National Academy of Sciences*, 116, 24433–24439. <https://doi.org/10.1073/PNAS.1908783116>
- Geyman, E. C., & Maloof, A. C. (2021). Facies control on carbonate $\delta^{13}\text{C}$ on the Great Bahama Bank. *Geology*, 49, 1049–1054. <https://doi.org/10.1130/G48862.1>
- Gierlowski-Kordesch, E. H. (2010). Chapter 1 Lacustrine carbonates. *Developments in Sedimentology*, 61, 1–101. [https://doi.org/10.1016/S0070-4571\(09\)06101-9](https://doi.org/10.1016/S0070-4571(09)06101-9)
- Gischler, E., Dietrich, S., Harris, D., Webster, J. M., & Ginsburg, R. N. (2013). A comparative study of modern carbonate mud in reefs and carbonate platforms: Mostly biogenic, some precipitated. *Sedimentary Geology*, 292, 36–55. <https://doi.org/10.1016/J.SEDGEO.2013.04.003>
- Gonfiantini, R. (1986). Environmental isotopes in lake studies. In *Handbook of Environmental Isotope Geochemistry, Volume 2: The Terrestrial Environment, B* (pp. 113–168). Elsevier.
- Gu, B., Chapman, A. D., & Schelske, C. L. (2006). Factors controlling seasonal variations in stable isotope composition of particulate organic matter in a softwater eutrophic lake. *Limnology and Oceanography*, 51, 2837–2848. <https://doi.org/10.4319/LO.2006.51.6.2837>
- Gu, B., Schelske, C. L., & Hodell, D. A. (2004). Extreme ^{13}C enrichments in a shallow hypereutrophic lake: Implications for carbon cycling. *Limnology and Oceanography*, 49, 1152–1159. <https://doi.org/10.4319/LO.2004.49.4.1152>
- Guo, L., & Riding, R. (1992). Aragonite laminae in hot water travertine crusts, Rapolano Terme, Italy. *Sedimentology*, 39, 1067–1079. <https://doi.org/10.1111/J.1365-3091.1992.TB01997.X>
- Havig, J. R., Hamilton, T. L., McCormick, M., McClure, B., Sowers, T., Wegter, B., & Kump, L. R. (2018). Water column and sediment stable carbon isotope biogeochemistry of permanently redox-stratified Fayetteville Green Lake, New York, U.S.A. *Limnology and Oceanography*, 63, 570–587. <https://doi.org/10.1002/LNO.10649>
- Helfrich, P., Ball, J., Berger, A., Bienfang, P., Cattell, S. A., Foster, N., Fredholm, G., Gallagher, B., Guinther, E., Krasnick, G., Rakowicz, M., & Valencia, M. (1973). *The Feasibility of brine shrimp production on Christmas Island*. University of Hawaii.
- Higgins, J. A., Blättler, C. L., Lundstrom, E. A., Santiago-Ramos, D. P., Akhtar, A. A., Crüger Ahm, A. S., Bialik, O., Holmden, C., Bradbury, H., Murray, S. T., & Swart, P. K. (2018). Mineralogy, early marine diagenesis, and the chemistry of shallow-water carbonate sediments. *Geochimica et Cosmochimica Acta*, 220, 512–534. <https://doi.org/10.1016/J.GCA.2017.09.046>
- Higley, M. C., & Conroy, J. L. (2019). The hydrological response of surface water to recent climate variability: A remote sensing case study from the central tropical Pacific. *Hydrological Processes*, 33, 2227–2239. <https://doi.org/10.1002/HYP.13465>
- Houghton, J., Fike, D., Druschel, G., Orphan, V., Hoehler, T. M., & Des, M. D. J. (2014). Spatial variability in photosynthetic and heterotrophic activity drives localized $\delta^{13}\text{C}_{\text{org}}$ fluctuations and carbonate precipitation in hypersaline microbial mats. *Geobiology*, 12(6), 557–574. <https://doi.org/10.1111/gbi.12113>
- Huson, D. H., Beier, S., Flade, I., Górska, A., El-Hadidi, M., Mitra, S., Ruscheweyh, H.-J., & Tappu, R. (2016). MEGAN community edition - interactive exploration and analysis of large-scale microbiome sequencing data. *PLOS Computational Biology*, 12, e1004957. <https://doi.org/10.1371/JOURNAL.PCBI.1004957>
- Ingalls, M., Frantz, C. M., Snell, K. E., & Trower, E. J. (2020). Carbonate facies-specific stable isotope data record climate, hydrology, and microbial communities in Great Salt Lake, UT. *Geobiology*, 18, 566–593. <https://doi.org/10.1111/GBI.12386>
- Ionescu, D., Spitzer, S., Reimer, A., Schneider, D., Daniel, R., Reitner, J., de Beer, D., & Arp, G. (2015). Calcium dynamics in microbialite-forming exopolymer-rich mats on the atoll of Kiritimati, Republic of Kiribati, Central Pacific. *Geobiology*, 13, 170–180. <https://doi.org/10.1111/GBI.12120>
- Jaramillo-Vogel, D., Foubert, A., Braga, J. C., Schaegis, J. C., Atnafu, B., Grobety, B., & Kidane, T. (2019). Pleistocene sea-floor fibrous crusts and spherulites in the Danakil Depression (Afar, Ethiopia). *Sedimentology*, 66, 480–512. <https://doi.org/10.1111/SED.12484>
- Kelley, C. A., Prufert-Bebout, L. E., & Bebout, B. M. (2006). Changes in carbon cycling ascertained by stable isotopic analyses in a hypersaline microbial mat. *Journal of Geophysical Research: Biogeosciences*, 111, 4012. <https://doi.org/10.1029/2006JG000212>
- Kelts, K., & Talbot, M. (1990). In M. M. Tilzer & C. Serruya (Eds.), *Lacustrine Carbonates as Geochemical Archives of Environmental Change and Biotic/Abiotic Interactions BT - Large Lakes: Ecological Structure and Function* (pp. 288–315). Springer Berlin Heidelberg. https://doi.org/10.1007/978-3-642-84077-7_15
- Kump, L. R., & Arthur, M. A. (1999). Interpreting carbon-isotope excursions: carbonates and organic matter. *Chemical Geology*, 161, 181–198. [https://doi.org/10.1016/S0009-2541\(99\)00086-8](https://doi.org/10.1016/S0009-2541(99)00086-8)
- Leng, M. J., & Marshall, J. D. (2004). Palaeoclimate interpretation of stable isotope data from lake sediment archives. *Quaternary Science Reviews*, 23, 811–831. <https://doi.org/10.1016/J.QUASCIREV.2003.06.012>
- van Heuven, S., Pierrot, D., Rae, J. W. B., Lewis, E., & Wallace, D. W. R. (2011). *MATLAB Program Developed for CO2 System Calculations*. ORNL/CDIAC-105b. Carbon Dioxide Information Analysis Center, Oak Ridge National Laboratory, U.S. Department of Energy, Oak Ridge.
- Lewis, E., & Wallace, D. (1998). Program developed for CO2 system calculations. *Ornl/Cdiac-105*.
- Londry, K. L., & Des Marais, D. J. (2003). Stable carbon isotope fractionation by sulfate-reducing bacteria. *Applied and Environmental Microbiology*, 69, 2942. <https://doi.org/10.1128/AEM.69.5.2942-2949.2003>
- Louca, S., Parfrey, L. W., & Doebeli, M. (2016). Decoupling function and taxonomy in the global ocean microbiome. *Science*, 353, 1272–1277. <https://doi.org/10.1126/SCIENCE.AAF4507>
- Lowenstam, H. A., & Epstein, S. (1957). On the origin of sedimentary aragonite needles of the Great Bahama Bank. *The Journal of Geology*, 65, 364–375. <https://doi.org/10.1086/626439>
- Maslin, M. A., & Swann, G. E. A. (2006). Isotopes in marine sediments. In *Isotopes in Palaeoenvironmental Research* (pp. 227–290). Springer.
- McCormack, J., Bontognali, T. R. R., Immenhauser, A., & Kwiecien, O. (2018). Controls on cyclic formation of Quaternary early diagenetic dolomite. *Geophysical Research Letters*, 45, 3625–3634. <https://doi.org/10.1002/2018GL077344>
- McCormack, J., Nehrke, G., Jöns, N., Immenhauser, A., & Kwiecien, O. (2019). Refining the interpretation of lacustrine carbonate isotope records: Implications of a mineralogy-specific Lake Van case study. *Chemical Geology*, 513, 167–183. <https://doi.org/10.1016/J.CHEMGEO.2019.03.014>
- McDougall, T. J., Barker, P. M. (2011). *Getting started with TEOS-10 and the Gibbs Seawater (GSW). Scor/lapso Wg127*.
- McMurdie, P. J., & Holmes, S. (2013). phyloseq: an R package for reproducible interactive analysis and graphics of microbiome census data. *PLOS ONE*, 8, e61217. <https://doi.org/10.1371/JOURNAL.PONE.0061217>
- Milliman, J. D., Freile, D., Steinen, R. P., & Wilber, R. J. (1993). Great Bahama Bank aragonitic muds; mostly inorganically precipitated, mostly exported. *Journal of Sedimentary Research*, 63, 589–595. <https://doi.org/10.1306/D4267B81-2B26-11D7-8648000102C1865D>
- Millo, C., Dupraz, S., Ader, M., Guyot, F., Thaler, C., Foy, E., & Ménez, B. (2012). Carbon isotope fractionation during calcium carbonate precipitation induced by ureolytic bacteria. *Geochimica et Cosmochimica Acta*, 98, 107–124. <https://doi.org/10.1016/J.GCA.2012.08.029>
- Morse, J. W., Gledhill, D. K., & Millero, F. J. (2003). Caco3 precipitation kinetics in waters from the great Bahama bank: Implications

- for the relationship between bank hydrochemistry and whittings. *Geochimica et Cosmochimica Acta*, 67, 2819–2826. [https://doi.org/10.1016/S0016-7037\(03\)00103-0](https://doi.org/10.1016/S0016-7037(03)00103-0)
- Newell, D. L., Jensen, J. L., Frantz, C. M., & Vanden, B. M. D. (2017). Great Salt Lake (Utah) microbialite $\delta^{13}\text{C}$, $\delta^{18}\text{O}$, and $\delta^{15}\text{N}$ record fluctuations in lake biogeochemistry since the late Pleistocene. *Geochemistry, Geophysics, Geosystems*, 18, 3631–3645. <https://doi.org/10.1002/2017GC007078>
- Nitti, A., Daniels, C. A., Siefert, J., Souza, V., Hollander, D., & Breitbart, M. (2012). Spatially resolved genomic, stable isotopic, and lipid analyses of a modern freshwater microbialite from Cuatro Ciénegas, Mexico. *Astrobiology*, 12, 685–698. <https://doi.org/10.1089/AST.2011.0812>
- Oni, O. E., Schmidt, F., Miyatake, T., Kasten, S., Witt, M., Hinrichs, K.-U., & Friedrich, M. W. (2015). Microbial communities and organic matter composition in surface and subsurface sediments of the Helgoland Mud Area, North Sea. *Frontiers in Microbiology*, 6, 1290. <https://doi.org/10.3389/FMICB.2015.01290>
- Orellana, L. H., Chee-Sanford, J. C., Sanford, R. A., Löffler, F. E., & Konstantinidis, K. T. (2018). Year-round shotgun metagenomes reveal stable microbial communities in agricultural soils and novel ammonia oxidizers responding to fertilization. *Applied and Environmental Microbiology*, 84(2), e01646-17. <https://doi.org/10.1128/AEM.01646-17>
- Parkhurst, D. L., & Appelo, C. A. J. (2013). Description of input and examples for PHREEQC version 3: a computer program for speciation, batch-reaction, one-dimensional transport, and inverse geochemical calculations. *Techniques and Methods*, 519. <https://doi.org/10.3133/tm6A43>
- Patterson, W. P., & Walter, L. M. (1994). Depletion of ^{13}C in seawater ΣCO_2 on modern carbonate platforms: significance for the carbon isotopic record of carbonates. *Geology*, 22, 885–888.
- Penger, J., Conrad, R., & Blaser, M. (2012). Stable carbon isotope fractionation by methylotrophic methanogenic archaea. *Applied and Environmental Microbiology*, 78, 7596–7602. <https://doi.org/10.1128/AEM.01773-12>
- Petryshyn, V. A., Juarez Rivera, M., Agić, H., Frantz, C. M., Corsetti, F. A., & Tripati, A. E. (2016). Stromatolites in Walker Lake (Nevada, Great Basin, USA) record climate and lake level changes ~35,000 years ago. *Palaeogeography, Palaeoclimatology, Palaeoecology*, 451, 140–151. <https://doi.org/10.1016/J.PALAEO.2016.02.054>
- Present, T. M., Gomes, M. L., Trower, E. J., Stein, N. T., Lingappa, U. F., Naviaux, J., Thorpe, M. T., Cantine, M. D., Fischer, W. W., Knoll, A. H., & Grotzinger, J. P. (2021). Non-lithifying microbial ecosystem dissolves peritidal lime sand. *Nature Communications*, 12, 1–8. <https://doi.org/10.1038/s41467-021-23006-1>
- Read, J. F. (1985). Carbonate platform facies models. *AAPG Bulletin*, 69, 1–21. <https://doi.org/10.1306/AD461B79-16F7-11D7-8645000102C1865D>
- Reimer, P. J., Bard, E., Bayliss, A., Beck, J. W., Blackwell, P. G., Ramsey, C. B., Buck, C. E., Cheng, H., Edwards, R. L., Friedrich, M., Grootes, P. M., Guilderson, T. P., Haflidason, H., Hajdas, I., Hatté, C., Heaton, T. J., Hoffmann, D. L., Hogg, A. G., Hughen, K. A., ... van der Plicht, J. (2013). IntCal13 and Marine13 radiocarbon age calibration curves 0–50,000 years cal BP. *Radiocarbon*, 55, 1869–1887. https://doi.org/10.2458/AZU_JS_RC.55.16947
- Richardson, C. M., Dulai, H., Popp, B. N., Ruttenberg, K., & Fackrell, J. K. (2017). Submarine groundwater discharge drives biogeochemistry in two Hawaiian reefs. *Limnology and Oceanography*, 62(S1), S348–S363. <https://doi.org/10.1002/lno.10654>
- Romanek, C. S., Grossman, E. L., & Morse, J. W. (1992). Carbon isotopic fractionation in synthetic aragonite and calcite: Effects of temperature and precipitation rate. *Geochimica et Cosmochimica Acta*, 56, 419–430. [https://doi.org/10.1016/0016-7037\(92\)90142-6](https://doi.org/10.1016/0016-7037(92)90142-6)
- Rosen, M. R., Turner, J. V., Coshell, L., & Gailitis, V. (1995). The effects of water temperature, stratification, and biological activity on the stable isotopic composition and timing of carbonate precipitation in a hypersaline lake. *Geochimica et Cosmochimica Acta*, 59, 979–990. [https://doi.org/10.1016/0016-7037\(95\)00016-X](https://doi.org/10.1016/0016-7037(95)00016-X)
- Saenger, C., Miller, M., Smittenberg, R. H., & Sachs, J. P. (2006). A physico-chemical survey of inland lakes and saline ponds: Christmas Island (Kiritimati) and Washington (Teraina) Islands, Republic of Kiribati. *Saline Systems*, 2, 1–15. <https://doi.org/10.1186/1746-1448-2-8>
- Saltzman, M. R., & Thomas, E. (2012). Carbon isotope stratigraphy. *The Geologic Time Scale*, 2012, 207–232. <https://doi.org/10.1016/B978-0-444-59425-9.00011-1>
- Schmitt, S., Conroy, J. L., Flynn, T. M., Sanford, R. A., Higley, M. C., Chen, M., & Fouke, B. W. (2019). Salinity, microbe and carbonate mineral relationships in brackish and hypersaline lake sediments: A case study from the tropical Pacific coral atoll of Kiritimati. *The Depositional Record*, 5, 212–229. <https://doi.org/10.1002/DEP2.71>
- Schneider, D., Arp, G., Reimer, A., Reitner, J., & Daniel, R. (2013). Phylogenetic analysis of a microbialite-forming microbial mat from a hypersaline lake of the Kiritimati Atoll, Central Pacific. *PLOS ONE*, 8, e66662. <https://doi.org/10.1371/JOURNAL.PONE.0066662>
- Scholle, P. A., & Ulmer-Scholle, D. S. (2003). A color guide to the petrography of carbonate rocks: Grains, textures, porosity, diagenesis. *AAPG Memoir*, 77, 1–486. <https://doi.org/10.1306/M77973>
- Singurindy, O., Berkowitz, B., & Lowell, R. P. (2004). Carbonate dissolution and precipitation in coastal environments: Laboratory analysis and theoretical consideration. *Water Resources Research*, 40, 1–12. <https://doi.org/10.1029/2003WR002651>
- Solari, M. A., Hervé, F., Le, R. J. P., Airo, A., & Sial, A. N. (2010). Paleoclimatic significance of lacustrine microbialites: A stable isotope case study of two lakes at Torres del Paine, southern Chile. *Palaeogeography, Palaeoclimatology, Palaeoecology*, 297, 70–82. <https://doi.org/10.1016/J.PALAEO.2010.07.016>
- Suarez-Gonzalez, P., & Reitner, J. (2021). Ooids forming in situ within microbial mats (Kiritimati atoll, central Pacific). *PalZ*, 95, 809–821. <https://doi.org/10.1007/S12542-021-00591-6>
- Talbot, M. R. (1990). A review of the palaeohydrological interpretation of carbon and oxygen isotopic ratios in primary lacustrine carbonates. *Chemical Geology: Isotope Geoscience Section*, 80, 261–279. [https://doi.org/10.1016/0168-9622\(90\)90009-2](https://doi.org/10.1016/0168-9622(90)90009-2)
- Talbot, M. R., Jensen, N. B., Lærdal, T., & Filippi, M. L. (2006). Geochemical responses to a major transgression in giant African lakes. *Journal of Paleolimnology*, 35, 467–489. <https://doi.org/10.1007/S10933-005-2828-Z>
- Talbot, M. R., & Kelts, K. (1990). Paleolimnological signatures from carbon and oxygen isotopic ratios in carbonates from organic carbon-rich lacustrine sediments. In *Lacustrine Basin Exploration: Case Studies and Modern Analogs* (pp. 99–112). American Association of Petroleum Geologists.
- Teranes, J. L., & Bernasconi, S. M. (2005). Factors controlling $\delta^{13}\text{C}$ values of sedimentary carbon in hypertrophic Baldeggersee, Switzerland, and implications for interpreting isotope excursions in lake sedimentary records. *Limnology and Oceanography*, 50, 914–922. <https://doi.org/10.4319/LO.2005.50.3.0914>
- Trower, E. J., Lamb, M. P., & Fischer, W. W. (2019). The origin of carbonate mud. *Geophysical Research Letters*, 46, 2696–2703. <https://doi.org/10.1029/2018GL081620>
- Valero-Garcés, B. L., Delgado-Huertas, A., Ratto, N., & Navas, A. (1999). Large ^{13}C enrichment in primary carbonates from Andean Altiplano lakes, northwest Argentina. *Earth and Planetary Science Letters*, 171, 253–266.
- Wong, H. L., White, R. A., Visscher, P. T., Charlesworth, J. C., Vázquez-Campos, X., & Burns, B. P. (2018). Disentangling the drivers of functional complexity at the metagenomic level in Shark Bay microbial mat microbiomes. *The ISME Journal*, 12, 2619–2639. <https://doi.org/10.1038/s41396-018-0208-8>
- Wyman, D. A., Conroy, J. L., Osburn, M. R., & Atwood, A. R. (2021). Coeval drying across the central tropical Pacific over the last millennium.

Paleoceanography and Paleoclimatology, 36, e2021PA004311.
<https://doi.org/10.1029/2021PA004311>

Zhu, T., & Dittrich, M. (2016). Carbonate precipitation through microbial activities in natural environment, and their potential in biotechnology: A review. *Frontiers in Bioengineering and Biotechnology*, 4, 4. <https://doi.org/10.3389/FBIOE.2016.00004>

SUPPORTING INFORMATION

Additional supporting information can be found online in the Supporting Information section at the end of this article.

How to cite this article: Chen, M., Conroy, J. L., Geyman, E. C., Sanford, R. A., Chee-Sanford, J. C., & Connor, L. M. (2022). Stable carbon isotope values of syndepositional carbonate spherules and micrite record spatial and temporal changes in photosynthesis intensity. *Geobiology*, 20, 667–689. <https://doi.org/10.1111/gbi.12509>